ACCESSIBILITY
Open

OsloMet – Oslo Metropolitan University

Department of Civil Engineering & Energy Technology
Section of Civil Engineering

Master Program in Structural Engineering & Building Technology

MASTER THESIS

TITLE OF REPORT **Mechanical behaviour and the modelling of PVC foam**	DATE 01.06.2022 PAGES / ATTACHMENTS 80/0
AUTHOR(S) Mojtaba Yosufzai, Eirik Westbye	SUPERVISOR(S) Professor Aase Reyes Associate Professor Jian Dai Professor Philippe Viot Dr Louise Le Barbenchon

SUMMARY / SYNOPSIS

The project study investigates the mechanical properties of a closed cell PVC foam material, Divinycell H80. Experimental tests have been done to characterize the intrinsic behaviour of the material. Afterwards a finite element analysis is done using a foam material model. Finally, the results from physical test are compared to those obtained from the finite element analysis.

KEYWORDS
PVC Foam
Divinycell H80
Experimental research
Finite Element Analysis

Abstract

Foam materials are widely applied in many industrial fields due to their superior characteristics regarding high strength to weight ratio. Additionally, they may offer high toleration to damage and exceptional energy absorption capacity. Therefore, a PVC foam of great mechanical performance, Divinycell H80, has been investigated in the current project report. First the mechanical properties of the foam are investigated by doing experiments, so that a good understandings of the behaviour of the material is established. Thereafter, a finite element analysis of the material was done to inspect the validity of the material model used.

In the project study the experiments done were compression tests and shear tests. The compression tests deemed viable results showcasing that Divinycell is an anisotropic foam. Additionally, it was confirmed that the mechanical strength of the material increases with increasing strain rate and foam density. Considering the shear tests, several shear tests were performed on the foam material, but the sample did not go through pure shear. This is investigated and analysed by using graphs, visual inspection and analysis software of the images taken during tests. After analysis of what happened during the tests, different modifications were made to both the sample and to the setup of the test. These modifications include reinforcing the sample with aluminium, making 3d-printed parts and CNC-manufactured parts for the test setup and investigation of the sample geometry and the effects of the changes. Lastly, an investigation is done of different articles that have found mechanical properties from shear tests with Divinycell or other materials in the past.

Finally, the compression results were modelled using the Deshpande-Fleck foam material model in LS-DYNA. This showed that the material model shows reasonable resemblance to physical compression tests performed, but densification occurs too early. However, the finite element model did not deform as wished, thus the results are looked at critically.

Preface

This project was conducted as a 30 credits Master's thesis project at Oslomet during the spring of 2022. The authors, Mojtaba Yosufzai and Eirik Westbye, were both students at the master's program Structural Engineering and Building Technology. During the project study about two months were spent in Bordeaux, France, to conduct physical experimentational work on a chosen material. Specifically, experimental research was done at the research institute Arts et Métiers using test-machines which they kindly let us use.

Acknowledgements

The authors would first of all like to greatly thank both our internal supervisors, Professor Aase Reyes and Associate Professor Jian Dai, and our external supervisors, Professor Philippe Viot and Dr Louise Le Barbenchon. We very much appreciate their thoughtful guidance and advice during the project study. Furthermore, we would like to extend our immense gratitude to the kind welcome and helpfulness given to us by our external supervisors, and not to mention the incredibly welcoming and nice researchers at the laboratory at Arts et Métiers, during our research stay in Bordeaux. Additionally, we thank Konnekt for funding in association with accommodation throughout the research stay in Bordeaux.

Abbreviations

FEM	Finite element model
FEA	Finite element analysis
PVC	polyvinyl chloride
CNC	Computer numerical control
DIC	Digital image correlation
D-F	Deshpande-Fleck

Nomenclature

Parameters	**Explanation**	**Unit**
E	Young's modulus	Pa
ρ_s	Density of bulk material foam is made of	kg/m^3
ρ^*	Density of cellular material itself	kg/m^3
σ	Stress	Pa
l	Cell edge length in foams	mm
t	Cell edge thickness in open-celled foams	mm
t_e	Cell edge thickness in closed-celled foams	*mm*
t_f	*Cell wall/face thickness in closed-celled foams*	*mm*
E_s	Young's modulus of the bulk material in the cell walls	Pa
E^*	Youngs modulus of the foam	Pa
φ	fraction of solid contained in the cell struts	*[-]*
ν^*	Poisson's ratio	*[-]*
ρ_0		*Kg/m^3*
Φ	yield function	
$\hat{\sigma}$	*Equivalent stress*	*Pa*
Y	*Yield stress*	*Pa*
σ_P	*Plateau stress*	*Pa*
$R(\hat{\varepsilon})$	*Representation of the strain hardening*	*[-]*
$\hat{\sigma}$	*Equivalent stress*	*Pa*
α	*Parameter describing shape of yield surface*	*[-]*
σ_m	*Mean stress*	*Pa*
σ_e	*Effective von mises stress*	*Pa*
ν_p	*Plastic poisons ratio*	*[-}*
p	*Hydrostatic pressure*	*Pa*
q	*Von mises stress*	*Pa*
p_c	*Hydrostatic compressive strength*	*Pa*
p_t	*Hydrostatic tensile strength*	*Pa*
σ_c	uniaxial compressive yield strength	*Pa*

Contents

List of figures

List of tables

1. Introduction

Polymeric foams are widely used in recent years as they are light and good at absorbing energy, while also having good properties for insulation [1]. In addition, the manufacturing process is easy, the foam is typically not expensive, and it is flexible when used in different designs. How the microstructure of the foam turns out depend on what the base material is and how the foam is manufactured. These factors affect the density, and the different mechanical properties as well as the thermal properties [2]. The main reason why foams are used as energy absorbers is due to a stress plateau region, where the cell walls of the foam buckle, making it able to withstand a large increase in deformation while the stress stays about same, until densification occurs[3]. Due to this, foams can be used as energy absorbers in vehicles and can protect building from blast and impact loads [4]. In order to predict the behaviour of foams as protective structures and energy absorbers, numerical models can be utilized. Furthermore, foams are used to protect humans against impact loads such as car crashes or against explosion load on buildings and that is why it is necessary to create accurate and trustworthy numerical models.

The behaviour of foams under different kind of loading is a complex process due to the microscopic structure of the foam [5]. However, existing material models can be utilized to replicate and represent this behaviour. The material models have different strength and weaknesses where the Deshpande fleck is an example of a material that is good because of the simplicity of the model. These material models are used in finite element software and in order to calibrate good models it is important to get a good understanding of behaviour under multiaxial loading for the material that is used. This understanding can be found through experimental testing of the material, and the knowledge can be used to improve the material models so that the behaviour accurately describes what is seen in the tests. The structure of foams makes it difficult to replicate the behaviour in a finite element program and is mainly due to foams consisting of pores, resulting in a volume change of the materials during loading. However, there are material models that take the volume change into account. A model developed by Deshpande and Fleck constitutively explains the behaviour of foams under multiaxial loading and material models used for foams can be based on this model [6]. By using material models in a finite element program, it is necessary to obtain mechanical properties for the material used. These mechanical data is found by doing different experimental tests on the foam, but the nature of the microstructure makes it challenging to perform certain tests.

In the current study, the main objective was to establish the mechanical properties of a polymeric foam, Divinycell, through experimental testing. The original objective was to perform compression tests, shear tests and hydrostatic test to obtain the necessary properties to input a material model in a finite element program. However, due to the existing challenges when performing the shear tests, the hydrostatic tests were not commenced. The focus shifted towards completing the shear tests to explain how the shear test on foam can be performed in order to get accurate graphs that can used to find the mechanical properties. What modifications can be done to the shear test setup and to the sample in the shear test

is explained in detail to help future research when performing the same tests. The modifications to the tests helped make the test more accurate, although more changes must be made to correctly establish the mechanical properties from the shear test. Using the data from the uniaxial compression test a number of different mechanical properties were established and input in the Deshpande-Fleck model in LS-Dyna. The remaining input data needed for the material model was gathered from other reports. Lastly a simulation that predicts the behaviour of an experimental verification test of Divinycell foam is presented and discussed.

1.1 Aim

The main goal of the project is to first do different experiments on the Divinycell H80 foam to get a good understanding of how the material behaves under different loads. The specific tests of interest are uniaxial compression tests, shear tests and hydrostatic compression tests. Additionally, if there is enough time some dynamic test on the material is wished to do. The microstructure of the foam is also of interest to investigate, thus taking pictures of this is also wished to do. After different tests are performed, finite element analysis is to be done to represent the behaviour which has been observed.

1.2 Method

To achieve this first a literature study is to be conducted on foam materials, and existing materials models for foams. During the study the mechanical behaviour of foams are specifically of interest. Next different possible material models which exist in FEM programs are to be looked into. This is so that one knows what type of material models are available to used based on achieved data from experimental testing. Additionally, the advantages and disadvantages of the material models are important to know, so that they are kept in mind when doing the finite element analysis. After the literature review different experimental tests are to be done on the foam material. Then the results are to be analysed, and finally a chosen test procedure is to be represented in a finite element analysis. With good understanding of the material it is wished to be able to deem the viability of a given material model, when used in regard to the Divinycell H80 foam.

1.3 Limitations

There are a set of limitations which occurred for the project. The first is the time aspect of the project which is constrained to the months between the first of January until the first of June. Thus, there is a time restriction given. Next is thethat time which was left for analysing results achieved from experimental tests were much less than anticipated. This is due to the problems which occurred with the shear test, making it so that solving that specific issue was the main priority. Thus, there are aspects of this project which were wished to be further investigated, but not possible due to much time going into working on experiments. Finally, it was very much wished to take pictures of the microstructure of the foam, but unfortunately the device for this did not work during the period of the experiments.

2. Theoretical background

In the following chapter a theoretical background is given to offer foundation to the work which is done in later chapters. Thus, theory of microcellular materials is presented, in addition to a more in-depth look at a specific type of industry microcellular material, Divinycell from DIAB [7]. Furthermore, models used to replicate the mechanical behaviour of foams are presented, along with some material models for microcellular materials used in finite element analysis programs today.

2.1 Introduction to microcellular materials

From Gibson and Ashby, a microcellular material, being a cellular solid, is defined as a solid made up of an interconnected network of solid struts or plates that form the edges and faces of cells [2]. Thus, one can have a material where there are open pore spaces. This leads to a large variety in the topology of the cell structure. Though, typically these are classified as two-dimensional arrays of cells, honeycombs, and three-dimensional arrays of cells, foams, as can be seen in figure 1 [2]. In three dimensions additionally there is the differentiation between cells that are interconnected, so that there is open space between the cells, and cells with membrane-like faces that are closed off from its neighbours. Leading to what is referred as open cell foams and closed-cell foams [8].

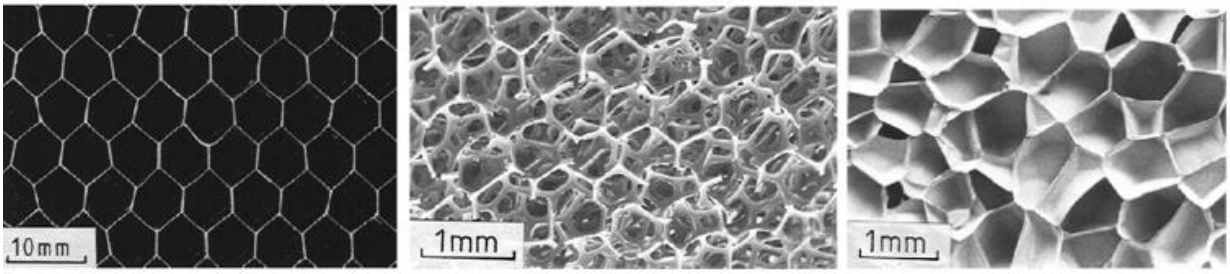

Figure 1: Examples of three typical microcellular structures, honeycomb(left), open-cell foam (middle) and closed-cell foam(right) [2, 9].

Great advantages with cellular materials are the abilities to be resilience, lightweight, stiff, high porous, and have good energy absorption capacities [10]. These factors depend on, among other things, the cell topology, the bulk material the foam is made of and the relative density of the foam [11]. The topology defines how the material is packed in space to form a porous material, while the bulk material the foam is made of gives the foam its intrinsic material properties. The relative density of a microcellular material is characterized as the ratio between the density of the cellular material, ρ^*, and the density of the bulk material from which the cell walls are made, ρ_s [12]. This is an important feature as it has a major effect on the modulus and compressive strength of a cellular material. Higher density foams have higher Young's modulus, yield strength and fracture strength [13].

Mechanical properties of foam

The mechanical response of foams to stress is greatly dependent on the solid material which the cell-walls of the foam are made of, though a common set of actions are to be observed. When a foam is

loaded in compression one can first observe linear elasticity at small stresses, followed by a plateau region, and finally a densification regime, as seen in Figure 2 [3].

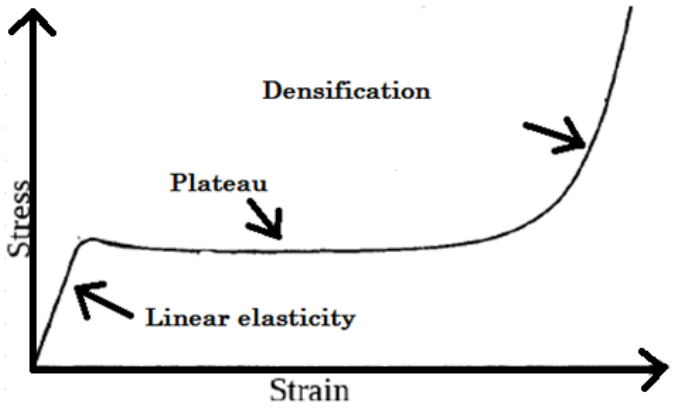

Figure 2: Example of a compression stress-strain curve for a foam [2]

At low stresses the foam behaves linearly with an initial slope equal to the Young's modulus, E^*, of the material. In this linear regime the elasticity is determined by cell wall bending in open-cell foams, and cell wall stretching in closed cell foams. After a certain point the foam reaches a yield stress in which the cells in the foam start to collapse and one can observe a stress plateau. This collapse may be caused by elastic buckling, plastic yielding or brittle crushing, depending on the bulk material the foam is made of. Once the cells in the foam have almost completely been crushed densification occurs, where opposing cell walls in the foam start to touch, and one can observe a rapid increase in stress with strain [14].

In the case where a foam is loaded in tension it has mechanical properties which resembles more that of a quasi-brittle material. The tensile response of a foam is such that it has a rapid increase in stiffness which ends in fracture, as seen in figure 3. Initially when loaded linear elasticity occurs due to cell wall bending, and cell wall stretching if the cells are closed. Then at larger strains the cell edges rotate toward the tensile axis, increasing the stiffness of the foam until fracture, for elastomeric and plastic cell wall material foams. In the case of brittle cell wall material foam a more sudden brittle crack occurs followed by failure. Compared to the compressive response for a foam, the tensile response is much stiffer, and not suited for large strains [2, 15].

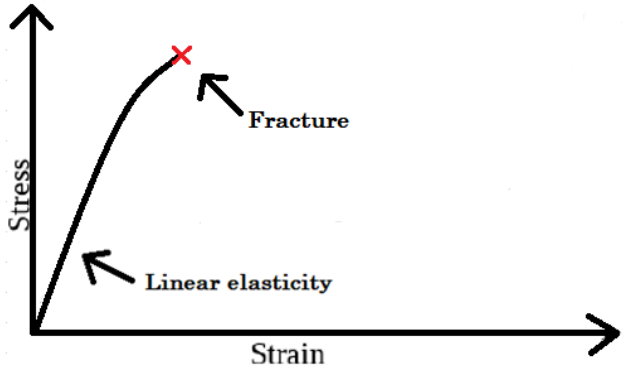

Figure 3:Example of a tension stress-strain curve for a brittle foam [2]

Fracture of foams

Foams experience fracture by cracking of the cell wall when testing in tension and shear. In tension the foams act linearly elastic before they experience brittle fracture and the same behaviour is observed when foams are tested in terms of shear [5]. The fracture and crack formations in foams is affected by the inhomogeneities of the foam. This inhomogeneity comes from the structure of the foam, where the foam consists of varying thickness of cell edges and cell walls. What is discovered from analysis of pictures of the microstructure of a foam during loading is that the cracks appear in the foam where the structure of the foam is the weakest. The cell edges and walls two main fracture mechanisms are necking followed by tearing [16].

2.2 Divinycell

Divinycell is a PVC-based material manufactured by DIAB that is primary used as a core material in layers with composite materials like polyester, vinyl ester or epoxy reinforces with glass, aramid, or carbon fibre. Divinycell is classified as a closed-celled foam and is often used as the core of sandwich elements because it is a strong, stiff, and light material. Additional beneficial properties of Divinycell is insulation and that it is water resistant due to the closed-cell structure [17-19].

2.2.1 How Divinycell is manufactured

Divinycell foams are produced by blending the raw ingredients together and then putting this mix in a mould. This mould in closed with clamps followed by a heating process in a press. When the heating process is done, the foam has become a solid slab. The slab is put in a hot bath and in this bath, it expands so that it reaches its density before it is cured. This is a process that makes the cells elongate, which affects the mechanical properties of the foam. Lastly, the material is divided into different sized sheets that is desirable for the different uses[20].

2.2.2 Physical properties of Divinycell

Divinycell foam is transversely isotropic, meaning that it behaves differently in one direction compared to the two other directions which behave isotropic. This is mainly due to the microscopic structure of the foam that was created during the manufacturing process. When manufactured, the cells grow more in the direction that is rising, creating pores that are bigger and elliptic in shape, in this direction. In the other directions the pores of the foam are discovered to be smaller and to have a round shape when studied in a microscope. Naturally, the direction with round pores is stronger due to it having less pore volume compared to the direction with elliptic shape pores. The direction with elliptically shaped pores is called the out-of-plane direction, while the two directions with round pores is the in-plane direction. Figure 4 shows the elliptic pores in the out-of-plane direction and the round pores in the in-plane direction. Because of the transversely isotropic nature of Divinycell it becomes harder to model in a finite element program [21, 22].

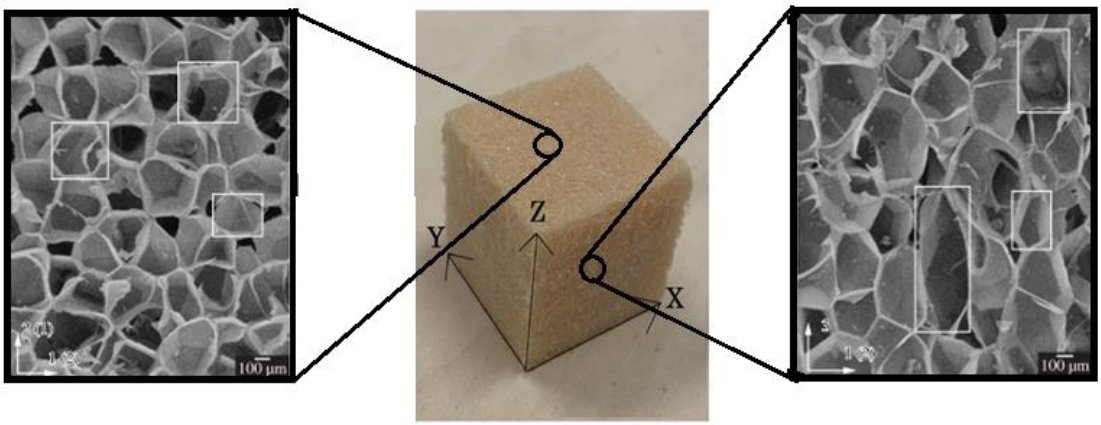

Figure 4 The microstructure of Divinycell foam, showing shape of pores in-plane and out-of-plane. The pore on the right is elliptic in shape and is in the out-of-plane direction. The pores on the left has a round shape and is in the in-plane direction [22].

2.2.3 Uses of Divinycell

The uses of Divinycell are many and it is used in several different industries because of the different properties of the foam. Divinycell can for example be used in the construction industry functioning as insulation, because of its density, porosity, moisture resistance and the thermal resistance of the material. In addition, it is used as supports of structures, due to the high strength of the material. It can also be used in a system with liquefied natural gas (LNG) as it resists hydrocarbons [19, 23, 24].

Because Divinycell has high strength and low weight, it is often used in transportation, offshore, wind power generation and civil engineering fields. Another good property for Divinycell is that the thermal conductivity can be reduced based on the ambient temperature. Divinycell is often used as the core of a sandwich elements, where a sandwich element is a structure that consists of three layers. In the core layer it is usually some low-density material, like Divinycell. The function of the sandwich structure is to resist in-plane bending and lateral bending loads with the panels of element, while the shear forces are mainly taken by the core of the element [19, 23, 24].

2.3 Modelling the mechanical behaviour of foams

To model and replicate how a foam material will behave mechanically can be a challenging task due to the microstructure of foams. The variability in density throughout a foam material, the topology and the effect of volume change are only a couple of factors which one may have to keep in mind. Based on this constitutive models have been developed for foams to predict how a given material may act under different type of loading. For the sake of illustrating this two different models are to be presented to see how some of these constitutive models function. These two models are the Gibson-Ashby model, and the Deshpande-Fleck material model.

2.3.1 The Gibson-Ashby model

One of the most generally accepted and used models for predicting the properties of microcellular materials are the models originally proposed by Gibson-Ashby [25]. In this case the mechanical

behaviour of open and closed-cell foams are described by representing the cell structure of a foam as an arrangement of cubic cells [2]. Both cases being visualised as presented in figure 5. Open-cell foams are characterized by members with edge length *l*, and edge thickness *t.* While closed-cell foams are also characterized by members with edge length *l*, and edge thickness t_e, but also include cell faces with a thickness of t_f. Neighbouring cells are then arranged such that their members connect at their mid-points.

The Gibson-Ashby foam model structure does not equate to how complex the geometric cell-shapes in real life foams are. Still, it does capture the same essential physical processes by which foams mechanically deform and fail [10]. This leads to the simplified cube structure being able to replicate the behaviour of a real foam by using scaling laws. The modelling of the mechanical behaviour of foams is different for open-cell foams compared to closed-cell foams. In open-cell foams the strength of the structure lies in the struts, as that is where all the solid bulk material resides. While in closed-cell foams there exists solid material both in the cell struts and the cell faces, thus the strength of the structure is affected by different components [26]. Next the linear elastic behaviour for open and closed-cell foams using the Gibson-Ashby model is to be presented, to showcase the differences. Specifically, parameters for compression are looked into as this is normally how foams are loaded.

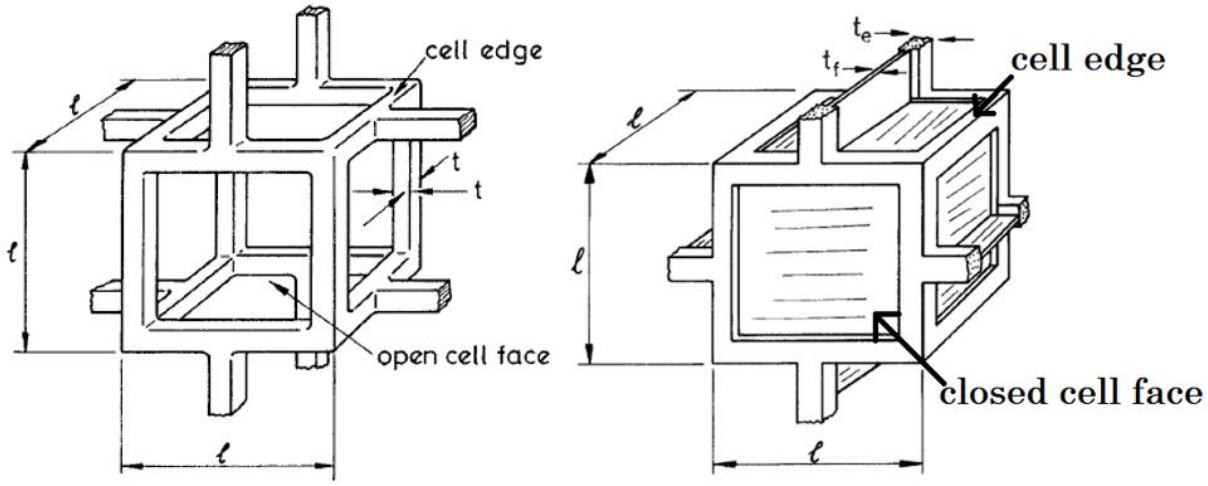

Figure 5: Open-cell foam Gibson-Ashby model (left), closed-cell foam Gibson-Ashby model (right) [2].

Elastic behaviour

For open-cell foams an estimation of the Young's modulus is derived by applying standard beam theory to the struts of the Gibson-Ashby cell structure. In this case one assumes that the elastic deformation of the struts, in regard to a load acting at the midpoint of the struts with length *l*, is related to the modulus of the structure [27]. For open-celled foams the Young's modulus is estimated by the formula as presented in equation 2.1 [11, 12]. Here, E^* is the Youngs modulus of the foam, E_s is the Young's modulus of the bulk material of the cell walls, and ρ^*/ρ_s is the relative density of the foam. The equation X predicts that there is a direct relationship between the relative density of an open-cell

foam, and its Young's modulus. It is important though to acknowledge that this modulus is at small strains.

$$\frac{E^*}{E_S} \approx \left(\frac{\rho^*}{\rho_S}\right)^2 \tag{2.1}$$

In the case of closed-cell foams one must include the contribution of solids which may be contained in the cell faces. Thus, if the fraction of solid contained in the cell struts is φ, then the remaining fraction which resides in the cell faces is defined as (1- φ) [2]. The inclusion of the cell faces makes it so that the Young's modulus for the closed-cell foam comes from three components. First is the bending of the cell walls, as for open-cell foams. Second component is the stretching of the cell faces, and the third component is the gas pressure inside the closed cells [26]. Thus, the Young's modulus for closed-cell foams including all these components is defined by Gibson-Ashby as seen in equation 2.2 [2, 27]. The formula consists of three parts where each one includes the effect of the components as mentioned. It can be observed that the Poisson's ratio, ν^*, of the foam is included for the inclusion of gas pressure. Again, it is important to note that this modulus is at small strains.

$$\frac{E^*}{E_S} \approx \varphi^2 \left(\frac{\rho^*}{\rho_S}\right)^2 + (1-\varphi)\frac{\rho^*}{\rho_S} + \frac{\rho_0(1-2\nu^*)}{E_S(1-\rho^*/\rho_S)} \tag{2.2}$$

2.3.2 Deshpande fleck material model

In order to model the behaviour of foams in a finite element program it is necessary to have a material model that is suitable for the material at hand. The Deshpande Fleck material model has proven to be a good model when dealing with different kind of foams, like for example aluminium foams and PVC-based foams like Divinycell [28]. This is because the model describes how materials act under multiaxial loading, taking hydrostatic loading into account. This is necessary for foams because a change in the volume occurs due to the cells of the foam collapsing under compression [5, 29]. The material model is fairly easy to use and has been in different reports to accurately model the behaviour of foams [5].

The yield criterion is similar to the Von-mises yield criterion, but in addition the Deshpande and Fleck yield criterion includes a parameter, α, that accounts for the volume change of the material. The yield criterion can be seen in equation 4 and is based on the yield function Φ in equation 3, where the equivalent stress $\hat{\sigma}$ is substituted [5, 29]. In equation 2.3 the Y is the yield stress and is expresses with the plateau stress, σ_p, and a representation of the strain hardening R($\hat{\varepsilon}$) where $\hat{\varepsilon}$ is the equivalent strain. In this yield criterion σ_e is the effective von mises stress. The σ_m is the mean stress, Y is the yield stress, while the α is a parameter that defines the shape of the yield curve. With α being 0 the von mises yield criterion is recovered. The equation for α alpha can be found in equation 4 [5, 29].

$$\Phi = \hat{\sigma} - \mathrm{Y} \tag{2.3}$$

$$Y = \sigma_P + R(\hat{\varepsilon}) \tag{2.4}$$

$$\hat{\sigma}^2 = \frac{1}{[1 + (\alpha/3)^2]}[\sigma_e + \alpha^2 {\sigma_m}^2] \tag{2.5}$$

$$\Phi = \frac{1}{\left[1 + \left(\frac{\alpha}{3}\right)^2\right]}[{\sigma_e}^2 + \alpha^2 {\sigma_m}^2] - Y^2 \leq 0 \tag{2.6}$$

$$\alpha^2 = \frac{9(1 - 2\nu_P)}{2(1 + \nu_P)} \tag{2.7}$$

The parameter ν_p is the plastic coefficient of contraction or the plastic Poisson's ratio. In the report from Deshpande-fleck, it is suggested that ν_p can be measured from a uniaxial compression test for a quick estimate of the value for α [29]. This way the shape of the yield surface can be found, meaning that the yield surface considers the volume change of the material. For an accurate representation of α it is best to measure ν_p when the uniaxial compression test has compressed the sample by 20-30% [5].

Figure 6 shows the yield surface of the model. To find it, different mechanical properties of the foam must be defined. The three inputs that are needed for defining this yield envelope in the hydrostatic pressure (p) and von Mises stress (q) space, include hydrostatic compressive strength (p_c) hydrostatic tensile strength (p_t) and uniaxial compressive yield strength (σ_c). In this way the elliptic yield-surface from the Deshpande and Fleck theory can be found [30].

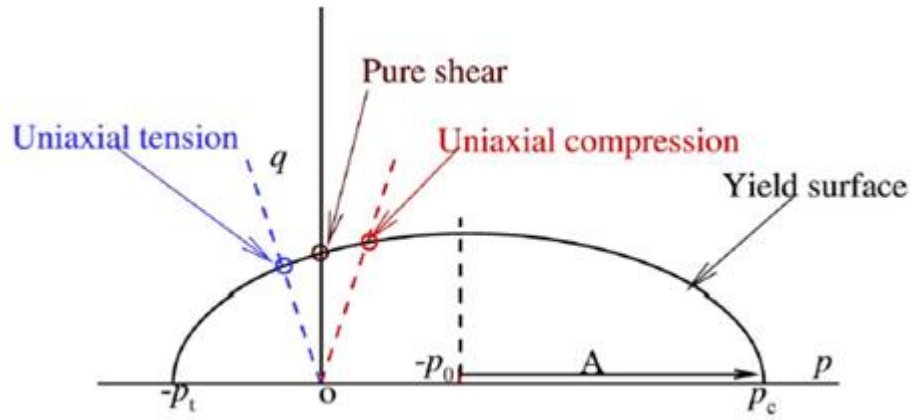

Figure 6 The elliptic yield surface of Deshpande-fleck model in the hydrostatic pressure (p) von Mises stress space (q) [31].

2.4 Available constitutive models for foam using numerical analysis

Numerical analysis is a method that uses algorithms to numerically approximate solutions to problems that otherwise are hard to solve with mathematical analysis. An example of this is the finite element method (FEM) which is a numerical method that is used to solve a mathematical formulation of a practical problem, by using differential equations. The way the finite element method works is by dividing a large problem into smaller problems. These smaller problems are referred to as finite elements, and by using approximations these problems are then solved [19, 32]. Examples of

commercially available FEM programs are LS Dyna and Abaqus, which both can model the behaviour of foams by using constitutive models [33, 34] . However, these models all have their own limitations and uses, and do not necessarily yield exact results in every context. Thus, a short introduction to some available constitutive models for foams which exist in LS Dyna and Abaqus are to be presented. Included are their uses and current disadvantages which may exist.

LS Dyna

When looking into material models for foams in LS Dyna there are many to choose from [34]. The choice of which one to use is dependent on the characteristics of one's foam during testing, and what the foam is planned to be used for [35]. Some examples of foam material models are the Low-density urethane foam model (MAT57), Fu-Chang's foam with rate effects model (MAT83), and the Deshpande-Fleck foam model (MAT154).

The Low-density foam model (MAT57) is used to model highly compressible foams, where one expects a high grade of recovery for the material. In this case the hysteresis and shape of the unloading and reloading force versus displacement curves in the elastic region can be controlled. Thus, loading and unloading behaviour is modelled. However, in the elastic region the evaluation of force and displacement, and residual deformation after unloading of the model can be improved [36]. Next, the Fu-Chang's foam with rate effects model (MAT83) may be used when it is wished to investigate the rate dependency effects on elastic foams. In this case the rate dependency can be found, however problems occur when one tries to account for unloading [35]. The Deshpande-Fleck foam model (MAT154) is an isotropic and continuum-based material model which includes fracture criteria and density variation in a foam. The model includes volume variation in foams, which is important as it is exhibited in for example metallic foams [37]. Based on the constitutive model developed by Deshpande and Fleck, it was implemented in LS Dyna by Reyes et al. and includes two criteria for fracture and statistical variation for foam density [5]. However, a constant shape of the yield surface is assumed, which is not always the case for foams, and rate dependency is not included in the model [38].

Abaqus

Considering the material models available in Abaqus some examples are Hyperfoam, Low Density foam and Crushable Foam [19, 39]. For the Hyperfoam model it's an elastomeric foam material model which is both isotropic and non-linear. The main use for it is instances where there are large volumetric changes, in compression up to 90% strain. Though, it is purely elastic, thus not suitable for foams which undergo permanent deformation [40]. The next model, Low density foam is mainly intended for low-density, highly compressible elastomeric foams which have significant rate sensitive behaviour. The model requires concrete specification of uniaxial stress-strain curves for both compression and tension at different strain rates. By using this data, it computes the stress by interpolation. However, this model assumes the Poisson's ratio of the material to be zero, though nonzero Poisson effects can be specified

thus including coupling along the principal directions. Still the models does not include negative Poisson-ratio [41]. The final model is the Crushable foam plasticity model, which is mainly intended for analysing crushable foams that are usually used as energy absorption structures. This is due to the fact that the model intends to model the cell wall buckling of foams which occurs due to compression. Additionally, it can model the difference between the foam in compression and tension. The material model has two different hardening models, where one is based on the isotropic hardening model developed by Deshpande and Fleck [19, 29]. Though, the model only looks into monotonic loading, and does not include the Bauschinger effect [42].

3. Experiments

A large part of the project itself is to characterize the mechanical properties of the closed cell PVC foam Divinycell H80 by doing experiments, in which specific mechanical properties are to be determined. Specifically, it was of interest to determine the parameters which are used in the Deshpande fleck foam model. To achieve this uniaxial compression tests, shear tests and hydrostatic compression tests were to be done. However, the shear tests proved to be more challenging to perform than anticipated, making it consume a lot of time and effort. Therefore, there was no time to perform the hydrostatic compression tests that initially were planned. Thus, the following chapter goes into detail on how the experiments were done to attempt to find specific mechanical material properties that were of interest, in addition to the results.

3.1 Manufacturing of samples and post processing of tests

3.1.1 Manufacturing of samples using CNC (Computer Numerical Control)

To make samples that can be used for experimental testing a different CNC-machines are normally used. CNC is short for Computer Numerical Control and is a term for machines that are used for manufacturing different parts. The machines are connected to computers that use a software where the geometry of the manufactured part can be made. An example of such software a is Fusion 360, which was used for the current study. Fusion 360 is a software from Autodesk that can be used to create different shapes in a 3D space. By connecting the software to a CNC-machine, the shapes made in the software can be cut by a CNC-machine out from different materials. The machines provide an accurate, and consistent manufacture process of parts or samples and is an efficient way to make samples. CNC machines are known for being accurate in manufacturing of parts and inaccuracies in the manufacturing of a sample is often due to human error [43]. In this thesis a CNC-machine called Shapeoko 4 was used and is seen in figure 7. This machine is known to accurately cut different type of materials. It can cut wood, soft metals like aluminium and it works very well for cutting Divinycell and other similar foams [44]. The accuracy of the produced parts is dependent on the operator of the machine, it depends on the different inputs in the software connected to the machine. Therefore, an experienced operator can usually provide more accurate manufactured parts. That being said, the software is easy to learn and with a small amount of training one can produce very accurate samples or parts.

Figure 7: The CNC machine which was used, the Shapeoko 4

3.1.2 Post processing test result data

The post processing procedure of test result data consisted of first investigating the force-displacement behaviour of the tests which was output from the test machine of choice. From the force-displacement data, stress-strain curves were extracted by calculating the nominal stress, σ, and true strain, ε, as seen in equations 3.1 and 3.2. Next, the Young's modulus is obtained by analysing the initial elastic part of the stress-strain curves obtained. The slope of the linear regime gives one the Young's modulus. The stress value which immediately follows after the elastic regime is deemed as the yield stress.

$$\sigma = \frac{F}{A_0} \tag{3.1}$$

$$\varepsilon = \ln\left(\frac{l_0 - l}{l}\right) \tag{3.2}$$

The Youngs modulus is found by from the stress-strain graph by finding the slope of the curve in the elastic part of the graph. When the rise is divided by the run the slope and the Youngs modulus is found, as is illustrated in figure 7.

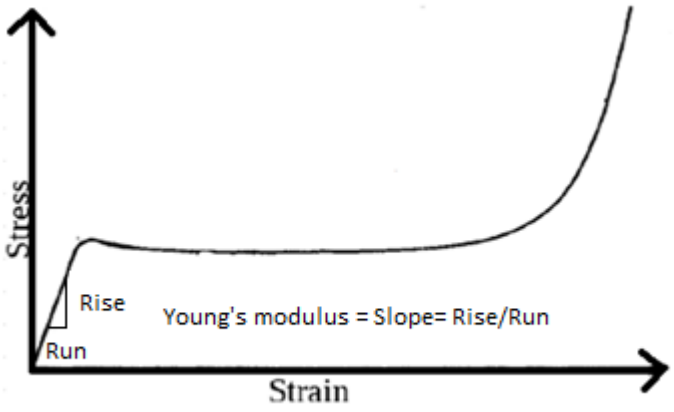

Figure 8 How the Young's modulus can be found from graphs [2]

DIC and GOM Correlate

To measure the displacement and strain field in certain mechanical tests a non-contact optical technique, Digital Image Correlation, is used (DIC). The method is based on using digital photographs of a component or test piece at different stages of deformation and comparing these. By doing this one can track blocks of pixels, thus the system can measure surface displacement and build up full field 2D and 3D deformation vector fields and strain maps. Digital Image Correlation (DIC) is a tool that can be used for finding the deformations and strain using pictures taken under experimental testing [45]. In analysing images with DIC it exists some inaccuracies. The results of the DIC are dependent on the image quality and the speckle patter that is applied to the sample and due to this the reliability of the analysis can be inaccurate. GOM Correlate is a software that uses DIC and is used in the current thesis to analyse images taken during tests. To track the relationship between the microstructure and mechanical

behaviour of the Divinycell H80 material, for the DIC, pictures were taken at a 1 Hz frequency with a Canon EOS 5D camera. Pictures were taken when tests at a machine speed of 5mm min^{-1} were done, and used later in correlation with DIC analysis.

When using GOM Correlate for analysis of the behaviour of the Divinycell foam, there exists inaccuracies in the current stud both because of inexperience of the program but mostly due to the speckle pattern that was created for the samples. The structure of Divinycell and the yellow colour makes it hard to apply a speckle patter of high quality. When the speckle pattern quality is evaluated by GOM Correlate it is mostly distributed in the area 1.00 to 3.00 where 10.00 is the best possible pattern quality, as seen in figure 8. The average pattern quality is around 2.70 which is not considered to be a reliable quality for accurate analysis of the images. A good pattern quality should be around 8.00 to 10.00. When analysing the results using GOM in the current study this must be taken into account when looking at the results.

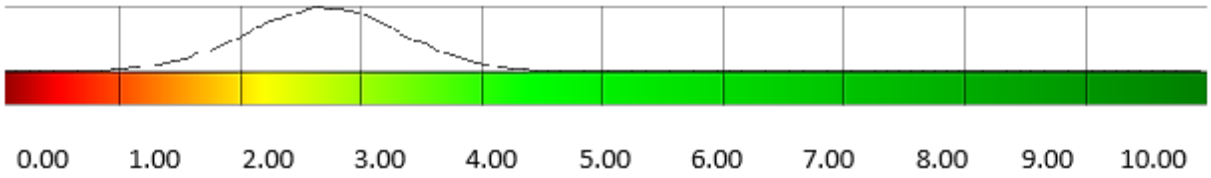

Figure 9 Distribution of pattern quality of the test specimen

3.2 Quasi-static uniaxial compression tests

3.2.1 Experimental setup and protocol

In the compression case study cube samples of Divinycell H80 were used with dimensions of 24x24x24 mm^3. The Divinycell H80 has an estimated density of 80kg/m^3 and relative density of around 0.057, as the density of PVC is assumed 1400 kg/m^3 [46]. The cube samples were obtained from a 35mm thick panel of Divinycell H80 and cut to cubes using a CNC machine, as seen in figure 9. To achieve this the 35mm panel was first placed in the CNC machine, which used a 3D model made in Fusion 360, and cut the top of the panel down to 24mm. Then using a different program in Fusion360 the CNC machine cut out squares of 24mmx24mm. Even though the samples have been cut by a machine, some uncertainty is to be expected for the dimensions because of human error. An example being, when cutting the top of the panel from 35mm to 24mm. Here the machine must be calibrated such that the drill is exactly at the surface of the panel, not any lower as it can damage the microstructure of a sample, and not any higher as the machine cuts down exactly 11 mm. Therefore, before doing any kind of testing the samples were first measured to get the volume of the sample, and weighed. Resulting in the density of each specific foam specimen being known. This showed that there was a density variation for the specimens, which is to be expected according to data from DIAB [7]. The effects of the density variation in the samples are to be investigated when looking at the results.

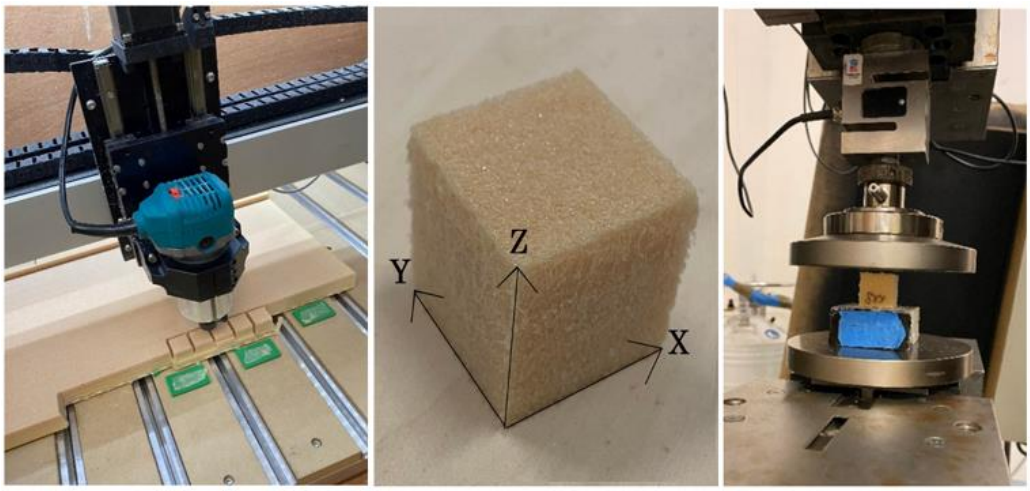

Figure 10: Picture of CNC machine cutting cubic samples(left), a 24mm cube specimen with assigned directions where Z is the foam rise direction(middle), and compression setup using the Zwick Roell Z250 strength testing device with a 10kN force sensor(right).

For the tests a compression machine, the Zwick Roell Z250 strength testing device from Allround-Line, with a 250kN load capacity was used. From literature studies [47, 48] it was known that a force higher than 10kN was not needed to compress the foam, thus also a 10kN force tensor was utilized with the machine to obtain more accurate results. Additionally, also based on literature studies [47, 48], a maximum deformation of 16mm, was chosen for the compression of the foam, such that one would have results for the linear elastic regime, the crushing phase, and only the initial parts of the densification phase. As the Divinycell foam is anisotropic the effects of this were investigated by using the two load directions, in-plane and out of plane, during the compression tests. Furthermore, the effects of the strain rate on the foam were evaluated by using two different strain rates. Thus, the loading speed for the machine was set to 5mm min^{-1} and 500 mm min^{-1}, which resulted in an average strain rate of $2.67*10^{-3}s^{-1}$ and $2.67*10^{-1}s^{-1}$, respectively.

3.2.2 Results and discussion

Low strain rate tests

In the case of the low strain rate tests, using a machine speed of 5mm min^{-1}, a total of 20 samples were tested. After measuring and weighing the samples it was discovered that a density variation from about 73kg/m^3 to 82kg/m^3 existed for these samples, as can be seen in table 1. Of the samples 7 were tested in the XY direction (in-plane direction), and 13 samples were tested in the Z direction (out of plane direction). The reason more tests were done in the Z-direction, than XY-direction, is because more instability was observed in the stress-strain graphs in this direction. Specifically, at the start of the densification regime of the material. The stress-strain results of all the 20 low strain rate compression tests are presented in figure 10. The graph includes both loading and unloading. From the graph one can observe that there is a difference in the mechanical behaviour of the samples. This is due to mainly due to the direction the specimens were loaded in, and the density variation of specimens.

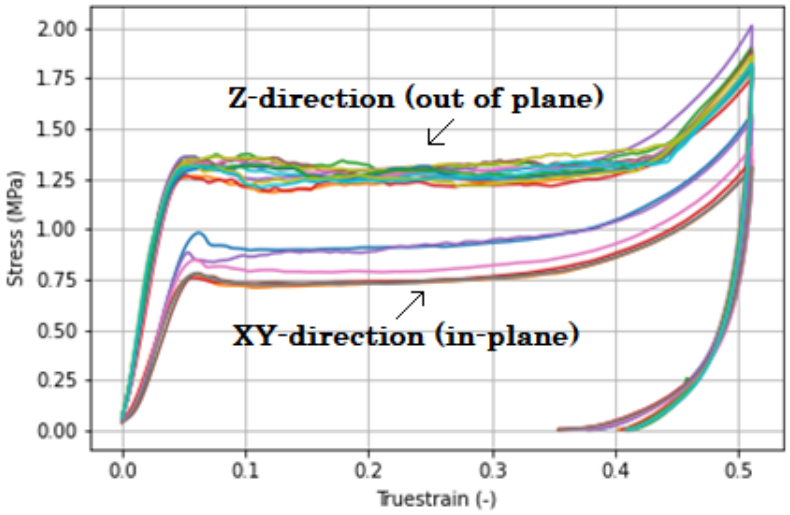

Figure 11: Stress-strain results of all 20 low strain rate compression tests done, the strain being expressed in true strain. The graph shows that the foam has weaker mechanical behaviour in the XY-direction compared to the Z-direction.

Sample name	*Height [mm]*	*Thickness [mm]*	*Length [mm]*	*Weight [g]*	*Load direction*	*Density[kg/m ^{3}]*
1	23,70	23,63	23,61	1,08	XY (In-plane)	**81,68**
2	23,70	23,85	24,03	0,99	XY (In-plane)	**72,89**
3	23,66	23,92	24,06	1,02	XY (In-plane)	**74,91**
4	23,78	23,72	23,75	1,07	XY (In-plane)	**79,87**
5	23,70	23,99	23,81	1,00	XY (In-plane)	**73,87**
6	23,93	23,92	23,76	1,03	XY (In-plane)	**75,73**
7	24,01	23,73	23,82	1,00	XY (In-plane)	**73,68**
8	23,95	23,68	23,74	1,00	Z (Out of plane)	**74,27**
9	23,99	23,67	23,69	1,00	Z (Out of plane)	**74,34**
10	23,87	23,76	23,72	1,02	Z (Out of plane)	**75,82**
11	24,32	23,61	23,53	1,06	Z (Out of plane)	**78,46**
12	24,57	23,48	23,56	1,06	Z (Out of plane)	**77,99**
13	23,70	23,67	24,08	1,08	Z (Out of plane)	**79,95**
14	23,88	23,74	23,65	1,01	Z (Out of plane)	**75,33**
15	24,10	24,07	24,06	1,06	Z (Out of plane)	**75,95**
16	24,05	24,08	24,10	1,05	Z (Out of plane)	**75,23**
17	24,04	24,08	24,17	1,08	Z (Out of plane)	**77,19**
18	24,04	24,12	24,03	1,05	Z (Out of plane)	**75,36**
19	24,06	24,13	24,11	1,05	Z (Out of plane)	**75,01**
20	24,15	24,06	24,04	1,05	Z (Out of plane)	**75,17**

Table 1:Table exported from Excel showing the dimensions and weight for each of the 20 samples tested at the machine speed of 5mm min -1. From the table it is observed that a variation of density from about 73kg/m3 to 82kg/m3 existed.

The effect of the anisotropic structural characteristics of the Divinycell foam is observed by analysing the results of the compression tests, as presented in figure 11. Presented are the two specimens, specimen 01 and 13, that each were loaded in a different direction. Both with densities near 80 kg/m^3, so that the density variation of the cubes would not be a factor. The results from the graph show that the material behaves different when it is loaded in the XY-direction compared to the Z-direction. The difference can for example be seen in the Young's Modulus, plateau stress and maximum stress of the specimens, as seen in table 2. The table shows that the material is stronger when loaded in the out of

plane direction than in the in-plane direction. Hence, it is concluded that the Divinycell H80 foam is a transversely isotropic material that is strongest in the out of plane direction.

	Density	*Young's Modulus*	*Plateau stress*	*Max stress*
*Test**01_XY**-Direction*	**81,7 kg/m^3**	**22,9 MPa**	**0,91 MPa**	**1,57MPa**
*Test**13_Z**-Direction*	**80,0 kg/m^3**	**36,4 MPa**	**1,32 MPa**	**2,01 MPa**
*Test**06_XY**-Direction*	**75,7 kg/m^3**	**18,1 MPa**	**0,79 MPa**	**1,34 MPa**
*Test**09_Z**-Direction*	**74,3 kg/m^3**	**30,2 MPa**	**1,27 MPa**	**1,83 MPa**

Table 2:Material and mechanical properties of the compression cube specimens 01, 06, 09 and 13, low strain rate compression.

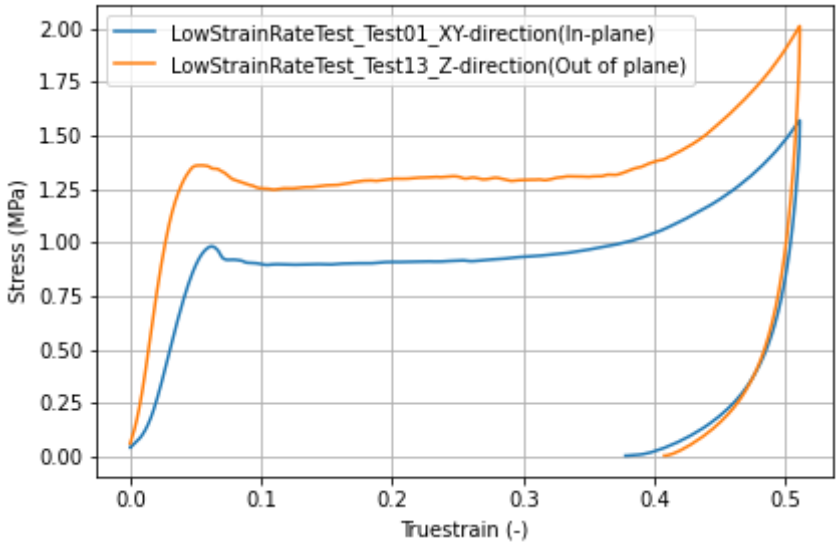

Figure 12: Quasi-static compression stress-strain graph for cube specimens 01 and 13, showcasing the effect of load direction.

The impact of the density variation of specimens was also investigated when analysing the results of the compression tests, as presented in figure 12. Presented are two stress-strain graphs, categorized by the load direction, each showing the behaviour of two specimens with different densities. Specifically, specimens 01, 06, 09 and 13. In both graphs there is a density difference of about 6 kg/m^3 for the specimens being compared. When comparing the impact of density variance, it is observed that samples with higher densities are stronger, as seen in table 2. The difference can for example be seen in the plateau stress and maximum stress of the specimens. However, this density difference is most impactful in the case where the specimen is loaded in the XY-direction. For loading in the Z-direction the most impact is observed for the maximum stress of the specimens, and little impact is observed for the plateau stress. Though, this is considered to be because of the instability which occurs in the plastic regime of the samples loaded in the out of plane direction. Longer cell edges in the out of plane direction result in more instability due to the plastic yielding of the cell edges. Thus, it is deemed that enough

experiments were not done to showcase the effect of small density variance in the out of plane direction. An increase in density should increase the strength of the material, in all directions.

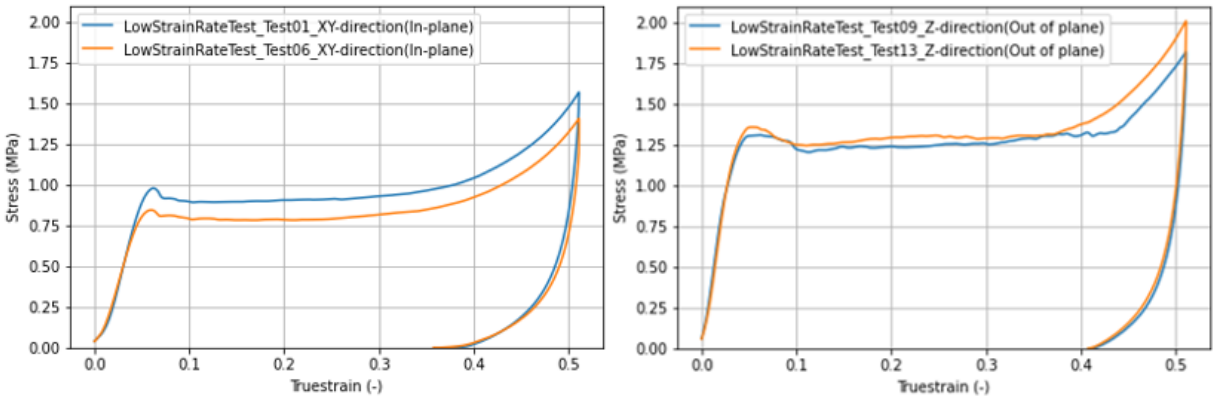

Figure 13: Quasi-static compression stress-strain graph for cube specimens 01 and 06 loaded in the XY-direction(left), and stress-strain graph for specimens 09 and 13 loaded in the Z-direction. Showcasing the effect of small density variance in test specimens.

High strain rate test and comparison

In the case of the high strain rate tests, using a machine speed of 500mm min $^{-1}$, a total of 17 samples were tested. After measuring and weighing the samples it was again discovered that a density variation existed for the samples. In this case a density variation from about 75kg/m^3 to 80kg/m^3 was to be observed, as can be seen in table 3. Of the samples 8 were tested in the XY direction (in-plane direction), and 9 samples were tested in the Z direction (out of plane direction). The stress-strain results of all the 17 high strain rate compression tests are presented in figure 13. The graph includes both loading and unloading. From the graph one can observe that there is a difference in the mechanical behaviour of the samples, the same as with the specimens loaded at lower strain rate. This again is mainly due to the direction the specimens were loaded in, and the density variation of specimens. As the effects of these factors have been investigated for the material already, it is chosen to only focus on the impact the strain rate has on the Divinycell H80 foam when going forward.

Even though these tests are called high strain rate tests, it must be mentioned that a machine speed of 500mm min $^{-1}$ is still considered a quasi-static test. Additionally, it is so that in the high strain rate compression tests less test values were registered in the machine, compared to the low strain rate compression tests. About 33% less test values were registered for the high strain rate tests, and this is due to the machine speed being faster. It can be observed in figure 13 by the graph curves being rounder, when for example looking at the maximum stress, compared to figure 10.

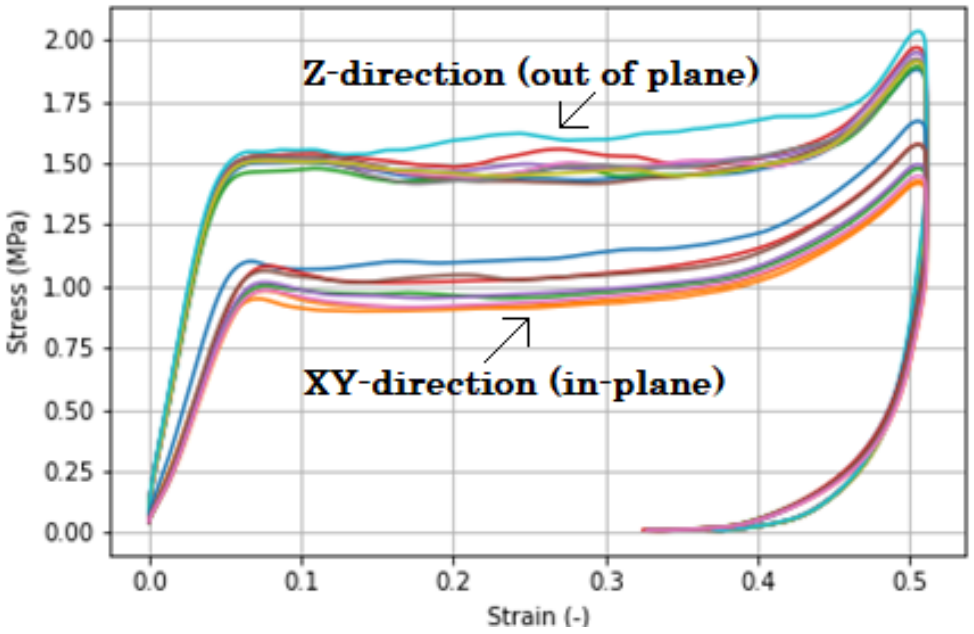

Figure 14: Stress-strain results of all 17 high strain rate compression tests done, the stress being expressed in true strain. The graph shows that the foam has weaker mechanical behaviour in the XY-direction compared to the Z-direction.

Sample name	*Height [mm]*	*Thickness [mm]*	*Length [mm]*	*Weight [g]*	*Load direction*	*Density[kg/m ^{3}]*
21	24,09	24,00	24,02	1,06	XY (In-plane)	**76,33**
22	24,02	24,24	24,09	1,11	XY (In-plane)	**79,14**
23	24,02	23,96	23,98	1,06	XY (In-plane)	**76,81**
24	24,02	24,05	23,97	1,09	XY (In-plane)	**78,72**
25	24,03	24,15	24,00	1,12	XY (In-plane)	**80,41**
26	23,97	24,05	23,98	1,09	XY (In-plane)	**78,85**
27	24,02	24,11	23,92	1,11	XY (In-plane)	**80,13**
28	24,08	24,05	23,93	1,07	XY (In-plane)	**77,21**
29	24,20	23,99	24,10	1,06	Z (Out of plane)	**75,76**
30	24,00	24,14	24,07	1,05	Z (Out of plane)	**75,29**
31	24,16	24,08	24,00	1,08	Z (Out of plane)	**77,35**
32	24,05	24,06	24,14	1,07	Z (Out of plane)	**76,60**
33	24,06	24,09	24,06	1,06	Z (Out of plane)	**76,01**
34	24,07	24,04	24,11	1,06	Z (Out of plane)	**75,98**
35	24,07	24,10	24,10	1,05	Z (Out of plane)	**75,11**
36	24,10	23,92	23,96	1,05	Z (Out of plane)	**76,02**
37	24,18	24,07	24,14	1,11	Z (Out of plane)	**79,00**

Table 3:Table exported from Excel showing the dimensions and weight for each of the 17 samples tested at the machine speed of 500mm min -1. From the table it is observed that a variation of density from about 75kg/m3 to 80kg/m3 existed.

The strain rate effects of the Divinycell H80 foam are observed when comparing the stress-strain relation of the foam in low strain rate tests with high strain rate tests, as seen in figure 13. Presented are two stress-strain graphs, categorized by the load direction applied on the foam, comparing specimens which were put under different strain rates. Specifically, specimens 01, 13, 25 and 37 were investigated as they have densities close to one another and therefore minimize the effect of small density variance. Ultimately the results show that an increase of strain rate results in an increase of mechanical strength

in the Divinycell H80 foam. This is visible when looking at the stress at yield point and plateau stress. Which can be observed both when loading the material in the in-plane direction and the out of plane direction, as seen in figure 14.

However, an uncertainty in the results is observed when looking into the Young's modulus. From table 4 the Young's modulus seems to be lower for the high strain rate tests compared to the low strain rate tests. This, based on literature studies, is known to be incorrect [14, 49]. When looking at the compared graphs from figure 14 it is observed that the Young's modulus is quite similar for the low strain rate tests and the high strain rate test. However, the low strain rate tests show an initial nonlinear part at low strains before the linear regime. Therefore, it is concluded that an error in calculating the Young's modulus of the foam has occurred, due to the way that the Young's modulus has chosen to be calculated in the project which includes the nonlinear initial part. Other experiments done on Divinycell foam show that the Young's modulus does not increase a substantial amount when the strain rate difference is as much as it is in the current project study [14, 49]. A higher difference in strain rate would showcase a clearer difference of the Young's modulus.

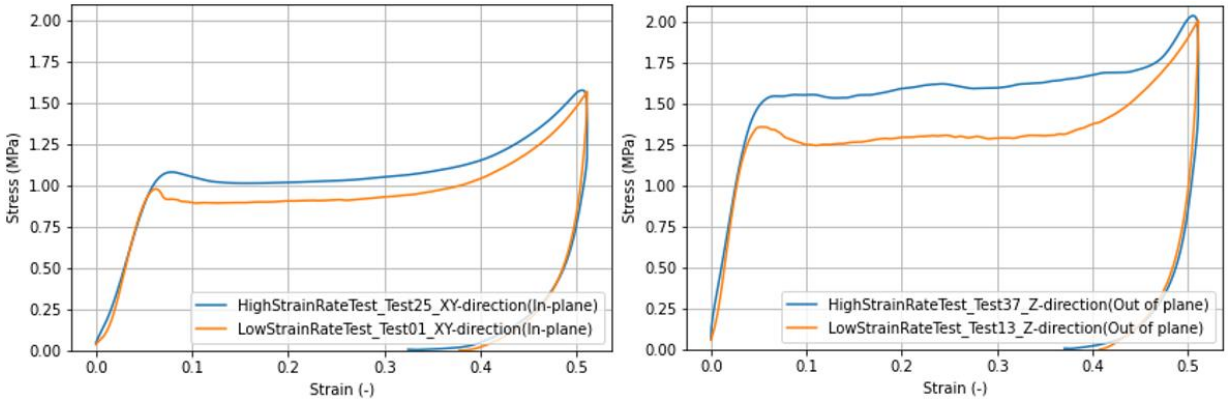

Figure 15:Compression stress-strain graph for cube specimens 01 and 25 loaded in the XY-direction with different strain rates(left), and stress-strain graph for specimens 13 and 37 loaded in the Z-direction with different strain rates(right)

	Density	*Young's Modulus*	*Plateau stress*	*Maximum stress*
*Test**01_XY**-Direction*	**81,7 kg/m³**	**22,9 MPa**	**0,91 MPa**	**1,57 MPa**
*Test**25_XY**-Direction*	**80,4 kg/m³**	**19,0 MPa**	**1,05 MPa**	**1,58 MPa**
*Test**13_Z**-Direction*	**80,0 kg/m³**	**36,4 MPa**	**1,32 MPa**	**2,01 MPa**
*Test**37_Z**-Direction*	**79,0 kg/m³**	**33,2 MPa**	**1,59 MPa**	**2,04 MPa**

Table 4:Material and mechanical properties of the compression cube specimens 01, 13, 25 and 37

Interestingly, the increase in strain rate has a larger impact when the Divinycell foam is loaded in the out of plane direction. From the table 4 it is observed that the difference in stress at yield point and plateau strength is higher when comparing the tests done in the Z-direction with those in the XY-direction. This is thought to be because the buckling of the cell struts is slower under higher strain rates. Therefore, this effect is amplified when the cell struts are longer, as the case is for the cell struts in the Z-direction. The buckling of cell struts is assumed slower under higher strain rated due to the way stress

propagates within the material, where the deformation of the material lags behind to a certain degree. One factor the strain rate does not affect much though is the maximum stress at the end of the 16 mm deformation, as observed from the figure 14. Concluded, it is observed that for the Divinycell H80 foam an increase in strain rate leads to an increase in the mechanical strength of the material. Additionally, the increase in strain rate has a higher impact when the material is loaded in the out of plane direction, compared to the in-plane direction.

3.3 Shear tests

Through shear testing of the material a greater understanding of the behaviour of the material is achieved. This chapter will describe the setup of the test, the sample that was tested and the procedure of the test. Originally the test was supposed to be a small part of the thesis to quickly establish the shear properties of Divinycell, but the shear test proved to be more difficult to perform than anticipated. Therefore, a big part of the research in Bordeaux became to figure out a way to get accurate graphs for the shear properties of the material by modifying the test setup and the shear sample.

3.3.1 Experimental setup and protocol

When preparing samples for the shear test, the CNC-machine was used to cut a shear sample that is referred to as a "butterfly-sample" because the geometry of the sample looks like a butterfly. The geometry of the sample is shown in figure 15 where the angle is shown to be 45 degrees and the radius is 1.585mm due to the manufacture process. Using a drill for the CNC-machine that is 3.17mm in diameter the smallest radius that can be cut is equal to the radius of the drill which is 1.585mm. Moving on this sample is used to successfully perform shear test on isotropic metals such as for example steel [50]. Before performing the shear tests the butterfly sample was put into a device that in this thesis is referred to as "L-shapes". The butterfly sample is placed inside the L-shapes as can be seen in figure 16. Then the sample is fastened by placing 4 metal cylinders that goes through the holes of the butterfly-sample and the L-shapes. Afterwards, the L-shapes were mounted in the compression machine by fixing the top part of the L-shape with a pin while the bottom L-shape stands on a compression plate. Finally, the shear tests were performed by moving the compression plate, making the bottom L-shape move upwards while the top L-shape was stationary.

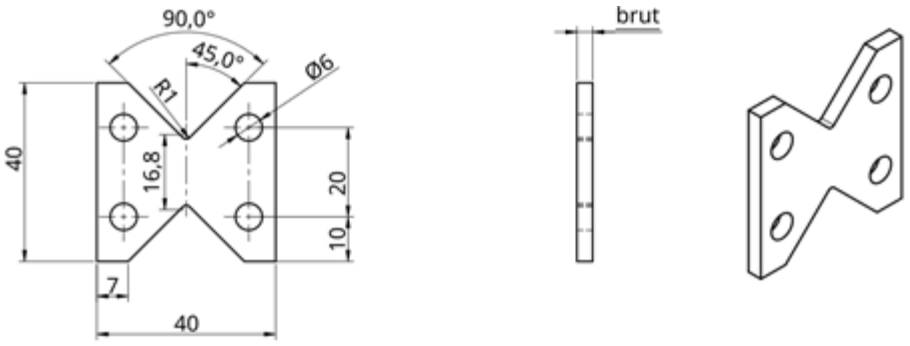

Figure 16:Butterfly-sample original geometry

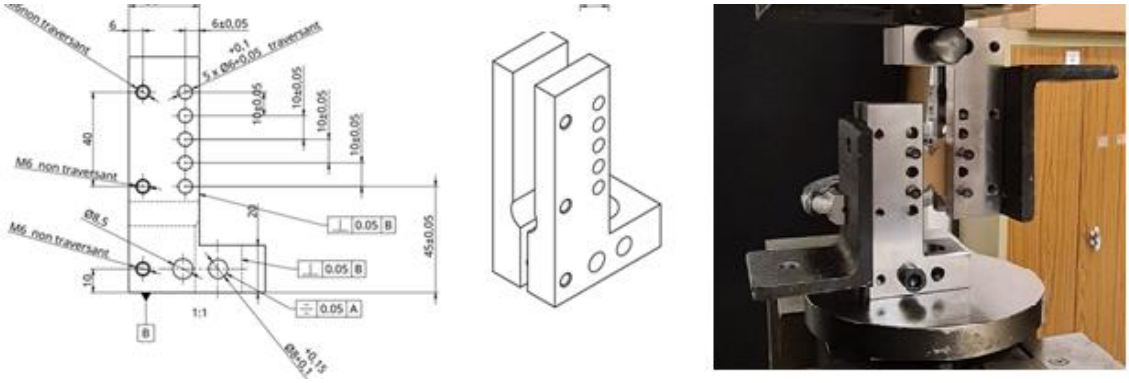

Figure 17:Geometry and illustrations of L-shapes (left), Butterfly-sample placed in L-shapes (right)

Test were conducted with the compression machine Zwick Roell Z250 that was described in the compression tests chapter. The loading speed was set to 5mm/min on all the tests, unless described otherwise. The maximum displacement was set to be 5mm, which was enough to see whether tests were successful, as most of the samples cracked before this displacement. The important part of the maximum displacement was to gather enough information about the behaviour of the sample during the tests, to later analyse the crack development with pictures and graphs. As Divinycell is transversely isotropic it needs to be testes in the in-plane and out-of-plane direction. However, in this thesis it was only tested in one direction to correctly perform a test in this direction before moving to the other direction. Another reason for not testing the sample in two direction was that the thickness of the divinycell sheet of which the samples were cut from was only 35 mm, while the thickness of the samples was 40mm. A change in the thickness of the sample is difficult because the rest of the setup is created for a specific thickness. The distance between the gap of the L-shape where the sample is put is 12mm, while the thickness of the sample was 6mm.

3.3.2 Modifications, results, and discussion of tests

When performing the tests, the middle part of the sample is supposed to shear in a straight line downward in order to go through pure shear and to have results that accurately describe the mechanical properties. However, when dealing with a foam like Divinycell, there exists some challenges when doing the shear test with this kind of setup and sample geometry. In that regard, changes had to be made to the test setup and the shear sample. This chapter will describe the different modifications that were made to the sample and to the setup, when trying to correctly perform a shear test on the material.

Initial test with original sample

When first performing the shear test with the original setup and the original sample, the sample would deform in the holes of the sample, and it would also rotate in the holes. In addition, the graphs in a force-displacement plane showed inconsistent results as can be seen in figure 17. By visual inspection during the tests and by looking at the inconsistency of the graphs, a modification of the sample was

needed. The shape of the blue graph is horizontally linear because the sample rotated in the holes. This rotation made the force stay more or less zero until rotation of the sample was no longer possible, and that is where the increase of force applied to the sample is observed. The thickness of the sample was a lot smaller than the gap in the L-shapes it was placed into, thus no friction was provided. That is why the thickness of the sample was increased to 11.5mm in an attempt to increase friction during loading, which prevents the rotation of the sample as observed in these tests.

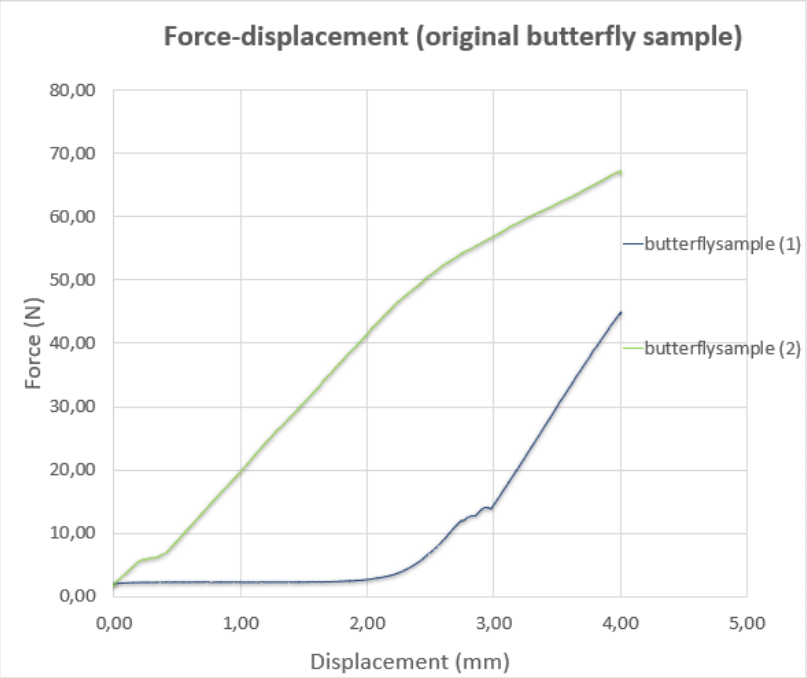

Figure 18:Force-displacement curve for the original butterfly sample. The two graphs show inconsistent behaviour of two samples with the same test setup and sample geometry

Reinforcement of the holes of the sample (glue and aluminium)

To prevent the holes of the sample from being the weakest part, two main methods of reinforcing the holes were used. First, glue was applied around the holes of the sample to make the holes more rigid. At the same time, the "wings" of the sample was made bigger, as can be seen in figure 18. This was done to have more material around the holes so that the holes would be less fragile. When testing the samples with glue as reinforcement, it was discovered that it was not sufficient as reinforcement around the holes. One of the reasons why glue was not a good idea could be because Divinycell is a closed-cell material, making the glue not enter the foam. This way the glue only laid on the surface of the sample, not creating sufficient reinforcement compared to if it would sink into the foams structure. The second approach was to reinforce the holes by making aluminium parts with the CNC-machine with the geometry that can be seen in the figure 18. These aluminium parts were glued on the wings of the butterfly sample seen in figure 21.

Figure 19:Sample with bigger wings and glue as reinforcement around the holes (on the left). Aluminium plates made by manufacturing with CNC-machine (on the right)

In order to glue the aluminium to the butterfly sample, it was necessary to create a setup that would apply pressure so that the sample and the aluminium parts would stick together. The device that was made included two wooden boards that would be on the bottom and the top of the sample with the aluminium parts, as seen in figure 19. On top of the upper wooden board a 25 kg weight was put to apply pressure. To prevent the samples from getting deformed two wooden prisms were made with the same height as the sample with the aluminium part and put beside the samples. The main purpose of the setup was to have metal cylinders in the holes of the sample and the holes of the aluminium part while the glue was drying. By doing this the holes of the aluminium parts and the holes of the sample was perfectly aligned. It is important to apply the glue carefully, as the glue was thin liquid at first before hardening and glue in the middle of the sample could make it stronger and cause inaccurate results when tested.

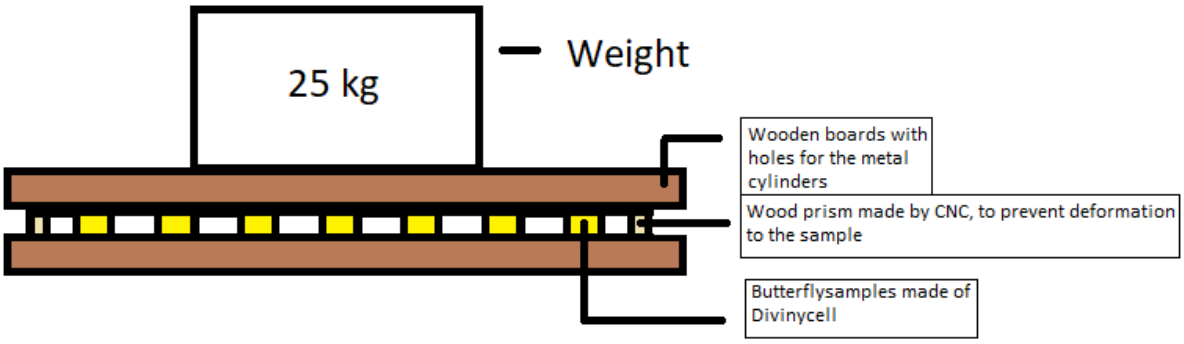

Figure 20:Sketch of the setup for gluing the aluminium parts to the sample

Figure 21:Wooden boards with holes made by CNC. One with metal cylinders (with plastic) and upper wooden plate (with soap)

Figure 22:The gluing process. On the left, a shear sample with aluminium on the top and bottom. In the middle, samples with aluminium on the bottom. To the right aluminium plates with glue.

Results

The shear test was carried out with the aluminium reinforced foam sample and the aluminium successfully served its purpose as reinforcement because the holes of the sample did not receive the same kind of deformation and cracks as before. However, the sample did still not go through pure shear. The cracks started to form in the middle, but instead of shearing straight down it went toward one of the holes of the sample as can be seen in figure 22. The graphs produced for the samples with aluminium reinforcement is presented in figure 23, and looks more promising in terms of the consistency of the graphs and due to shape of the graph when compared with other articles [30, 51]. The variation of the graphs could be due to the variation of density of the different samples. The density of the shear samples was not measured in these tests because the main goal was to make the shear setup better in terms of shearing the sample in the middle. Therefore, analysis of the variation of density is considered unimportant when investigating the general crack pattern of these tests.

Figure 23:Crack development of sample with aluminium reinforced holes

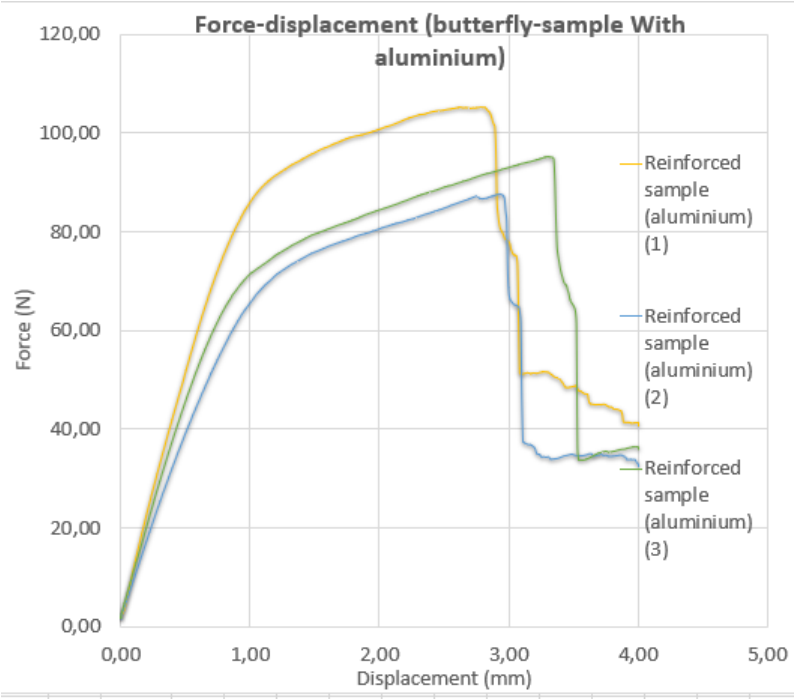

Figure 24: Graphs from shear tests with aluminium reinforcement. The yellow, blue, and green graphs are samples that have the same setup and the same geometry.

However, the sample did not go through pure shear due to the crack development in the sample, and therefore different theories were made to find the root of the problem. The main theory about why the cracks formed like this was believed to be because of rotation during the shear test. Another possibility could be that the middle part of the sample was too strong, making it harder to crack. In addition, some deformation could occur before testing while being produced by the CNC. Lastly, deformations could also easily happen due to the handling of the sample when mounted in the shear testing equipment, making small imperfections in the foam. To make the handing of the sample easier when put into the shear equipment a plastic plate was made that could be fastened to the two L-shaped aluminium parts, making them rigid and act as one part. This way the sample would not receive any deformations while put into the compression machine. For the following tests the plastic plate is used as a part of the setup in all tests. The plastic part is seen in figure 24. In table 5 an overview of the challenges regarding the test are presented and possible solutions made to them. The solutions are later described in more detail.

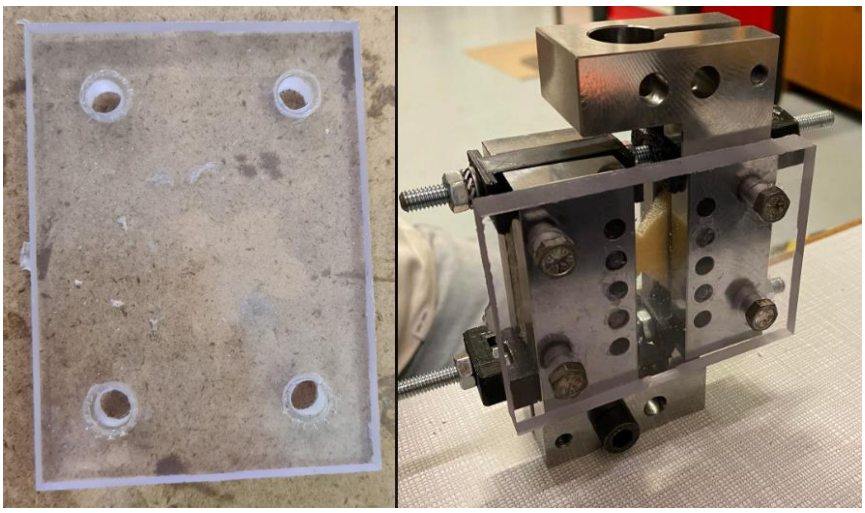

Figure 25: CNC-manufactured plastic part added to the setup of the shear test

Possible reasons why tests are unsuccessful	Modification to sample or setup
The sample could be too thick in the middle	Reducing thickness in the middle part of the sample
Deformation due to handling of the sample	Manufactured plastic plate to make the system rigid
Problem with the geometry	Different geometries of the sample were made with change to radius and angle of the sample
Rotations due to moment	Analysis of the pictures show bottom L-shape moving closer to the top L-shape during testing. There for devices are made to keep the same distance during the tests.

Table 5:Overview of existing problems and possible solution to them

Reducing cross-section of samples

Because one theory was that the sample was too strong in the middle, new samples were made with a smaller thickness in the middle. The reduced thickness in the middle was cut out by the CNC-machine on one side before it was turned around to the other side and cut there too. Because the samples had be turned to reduce the thickness on both sides it exists some inaccuracies. This is because it is hard to turn the sample so that it is in the exact same position as before it was turned. The sample with reduced cross-section can be seen in figure 25. To see the effect of the reduced cross-section and to further analyse what happens during the shear tests, speckle pattern was applied to the samples with reduced cross-section and to samples with no reduction in cross-section.

Figure 26: Bottom sample with 8mm thickness. Top sample with 4mm thickness

Results

Although the cross-section was reduced, the sample cracked the same way as the sample with no reduction in thickness and can be seen in figure 26. The graphs for the samples with a reduction in cross-section is presented in figure 27. The graphs show three curves where the blue and the yellow curve is samples with 4,5mm in thickness, while the grey graph is for a sample with 4mm in thickness. When these graphs are compared to the graphs with the original 8mm cross-section, they are naturally weaker in terms of the amount of force it can withstand and the displacement it can take before fracture. The blue and yellow curves should be more or less similar, but the blue is a good bit stronger than the yellow. The difference in strength is considered to be too much to be because of the density alone. One probable reason why the difference is this big between the two is because of initial deformation when handling the samples before the tests. Further analysis of the pictures from the tests can help under the graphs better.

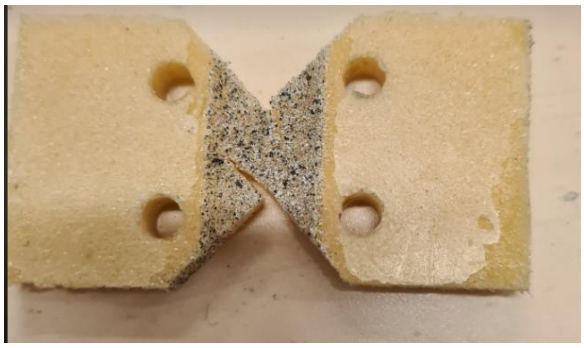

Figure 27: Cracked sample with speckle pattern

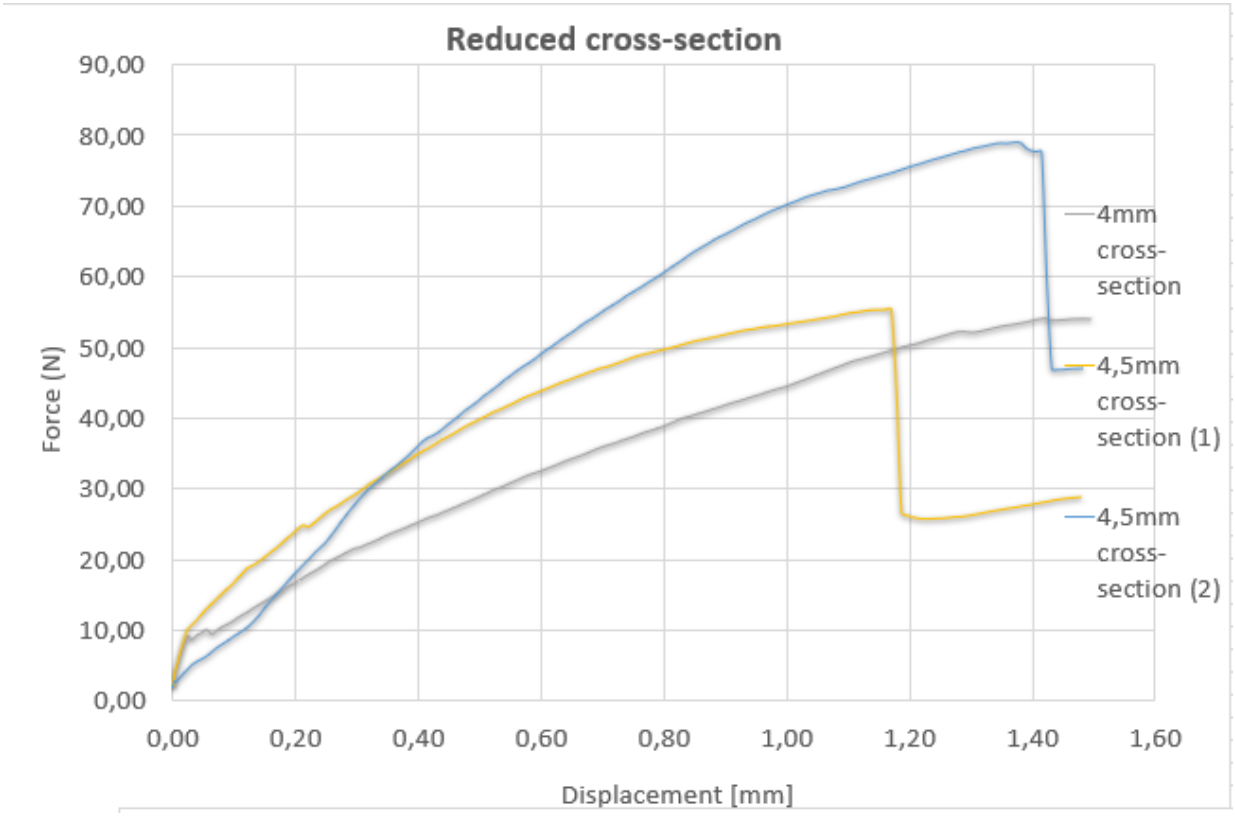

Figure 28:Graphs showing Force-displacement curves of samples with smaller cross-section. The blue and yellow graphs is for sample with thickness 4,5mm in the middle, while the grey graph is for a sample with 4mm thickness in the middle.

When analysing the images after the tests, it seemed like the moving L-shape moved closer to the stationary upside down-L in the lateral direction. By the images it looked like the cells of the foam moved closer together in the opposite side of part that was moving, believed to make the foam locally stronger. While the opposite happened for the side of the butterfly sample that was pushed upwards, where the cells moved further apart making the material weaker on this side. This made the sample crack on the side that became weaker. By using GOM-correlate it became easier to see that the moving L-shape, moved not only in the z-direction, but also in the x-direction seen in figure 28. In the figure the sample is rotated 90 degrees, meaning that the y-direction in the figure in the x-direction in reality. This is believed to create a moment and could be a reason why the cracks start in the middle and moved toward a hole. Figure 28 shows only the positive displacement during loading in the undeformed state and the deformed state before cracks appear. It is observed by these images that the bottom right corner is moves in the positive y-direction during the tests. This is believed to be because the L-shape that is moving is pushing the top left corner against the other L-shape this results in the displacement of the bottom right corner.

Figure 29 shows the undeformed state of the sample before loading and the deformed state of the sample before cracks appear. In the figure the grid is placed in the same place for both cases and in the deformed image one side is elongated while the other side is shortened when using the grid as a reference. Therefore, it is suggested that it crack towards the side that is elongated because the cell in

the foam is stretched compared to the other side where the cells are believed to be compacted, making it stronger.

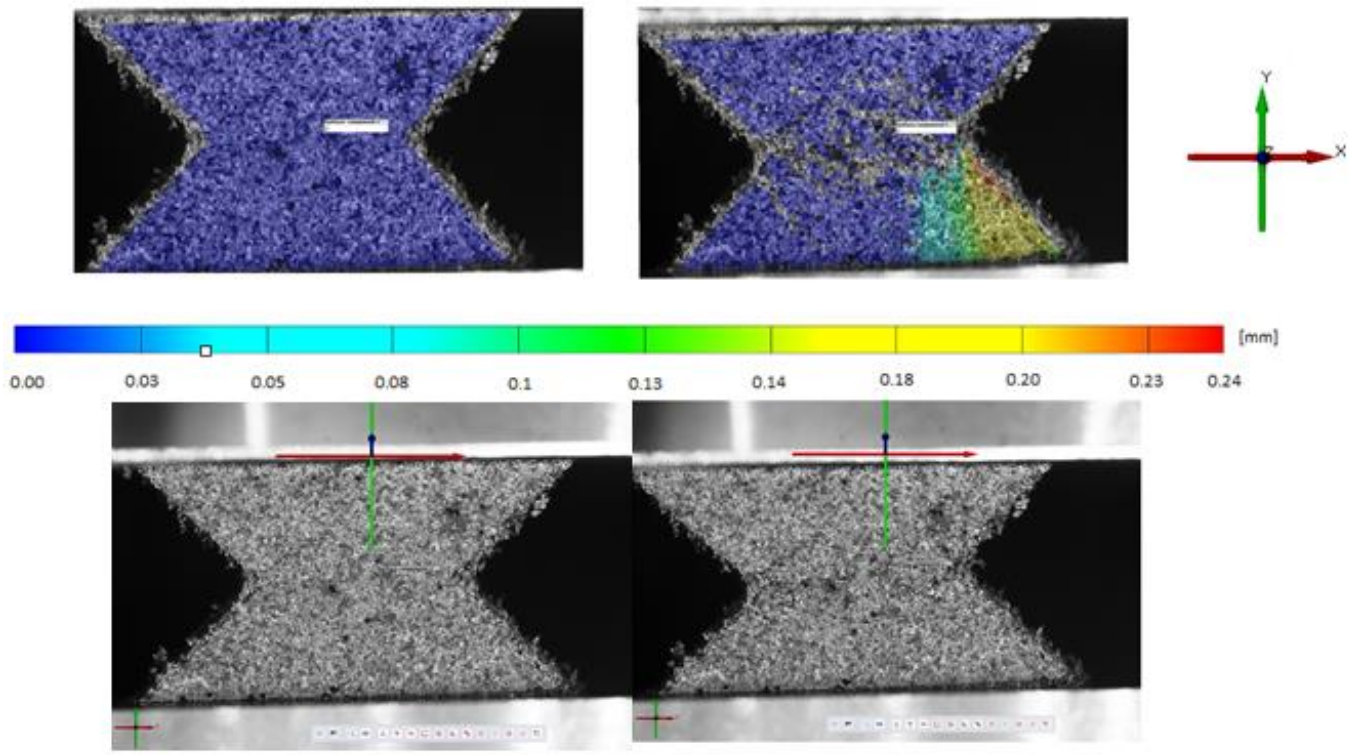

Figure 29:Displacement in y-direction showing that the bottom right corner of the sample is moving toward the L-shape that is moving.

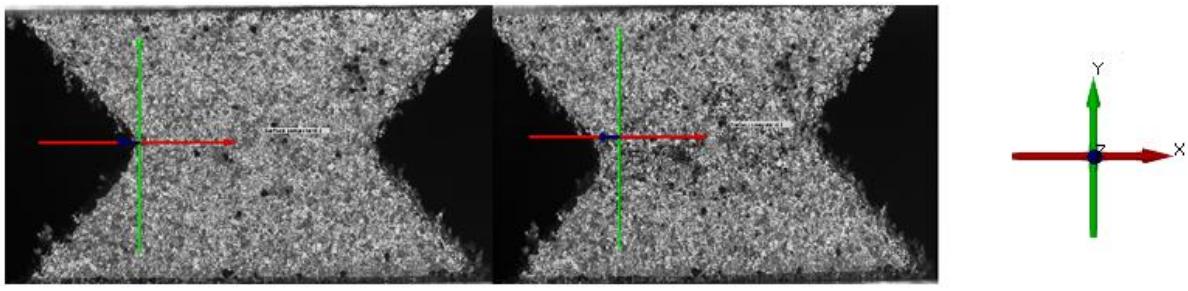

Figure 30:Picture showing the undeformed state of the sample before test and the deformed state before cracks appear.

Change of the setup with 3d-printed devices

To keep the same distance between the L-shapes during the tests, devices were created. Using a 3d-printer, plastic parts were made to fit into the L-shapes and the plastic parts contained a hole that a screw could be screwed into. The devices can be seen in use in figure 30. With these 3d-printed devices new tests were done on the aluminium reinforced butterfly-samples with no reduction in cross-section and butterfly-samples with smaller thickness in the middle.

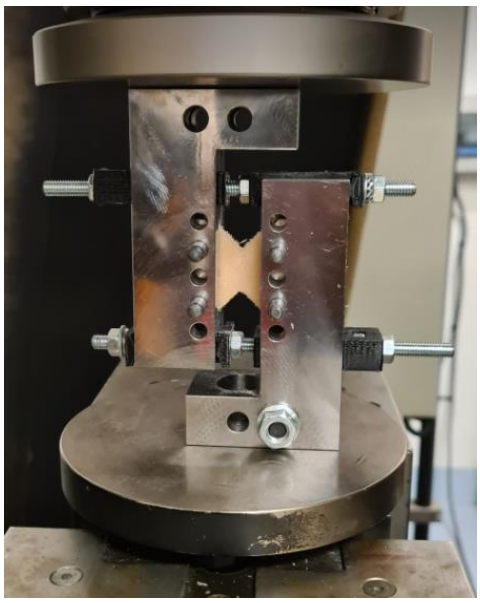

Figure 31: Shear test with 3d-printed devices keeping the distance between L-shapes

Results

The formation of cracks in the samples seemed similar to the previous tests without the 3d-printed devices. However, when looking at the images during testing the 3d-printed devices had served its purpose and the distance between the L-shapes did not change during the test and is seen in figure 31. In this figure there an image of the undeformed state and an image of the cracked state during testing is included. The axis is placed on the same point on each image and shows that the x axis is aligned with the L-shape the entire time during testing, proving that the distance between the L-shapes is the same. The reason why it did not go through pure shear is in this case is unknown, but one theory could be because of the nature of the foam. Because the foam consists of pores, differences in relative density can make the foam weaker in certain parts of the foam. When the cracks start to form it is more likely to crack towards the parts of the foam that has more pores and less material. This is considered to be an unlikely theory because the large number of tests that all crack in more or less the same manor. Ideally, the L-shapes would be pulled apart from each other to avoid rotations, but due to equipment restrictions it was not tried this way.

The graphs from the samples with the new setup with 3d-printed devices is shown in figure 32. All graphs show samples with aluminium reinforced holes and a thickness of 8 mm. The difference in the graphs is believed to be somewhat because of the density, but also because slight differences in the setup of the tests. The grey graph represents a sample that after a certain point received extra strength because the 3d-printed devices took a lot of the force because of wrongly setting up the devices. Some inaccuracies exist when using these devices could offer more strength to the devices because of friction force when the plastic is sliding through the gap in the L-shapes.

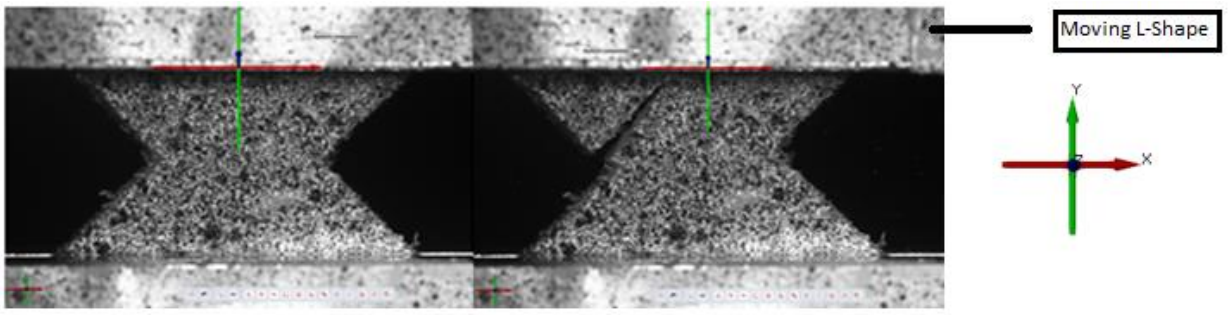

Figure 32:Image showing that the distance between the L-shapes is the same during the shear test of the sample. To the left a picture of the undeformed sample and to the right a picture taken immediately after the crack appeared.

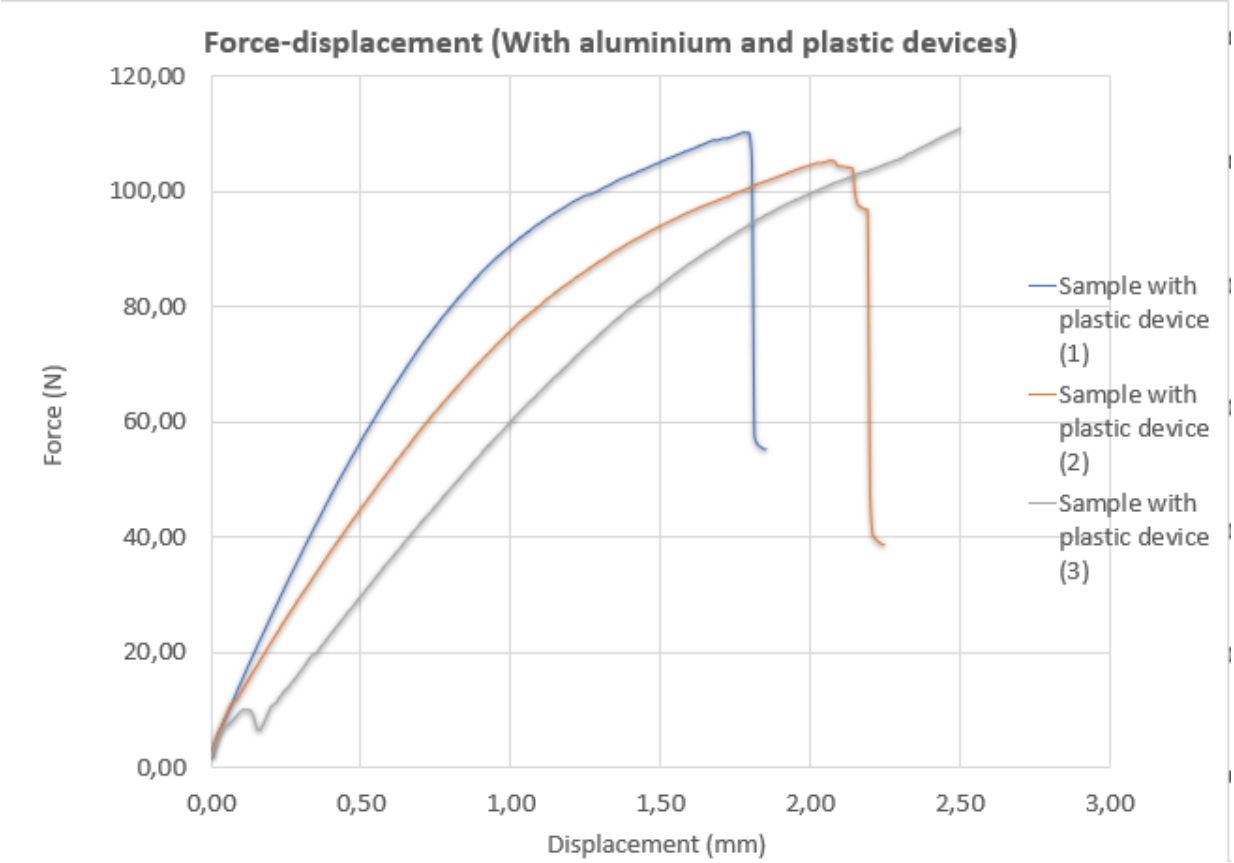

Figure 33:Graphs showing Force-displacement curves of tests done with plastic devices. All the curves is obtained using the same sample geometry.

Investigation of different sample geometries

To investigate whether a change in the geometry of the sample could make it easier to shear the sample in the middle different samples were made. The changes in the geometry from the original samples were made to the angle and the radius. The original sample had an angle of 45 degrees and a radius that is 1.585mm. The different radiuses that were investigated were: 0, 5 and 10, while the different angles in degrees were: 50, 45, 15 and 0. Samples were made combining these radiuses and degrees. For example, a sample with 50 degrees would be made with 0, 5 and 10 in radius. All the previously mentioned degrees would be combined with these radiuses. An overview of the different radiuses and the different angles is presented in table 6.

Angle [degrees]	Radius [mm]
0	0
15	1.585
45	5
50	10

Table 6: Overview of the radiuses and the angles that are combined to make different samples

Samples with 0- and 15-degree angles

First the sample with 0 degrees were manufactured and tested. When tested, it was found that the cracks started to form in the top right hole of the sample. Due to it having the same thickness in middle of the sample as the rest of the sample, the weakest part became the holes. The same was the case for the samples with 15 degrees combined with the different radiuses. These samples have too much foam material in the middle, making the holes the weakest part of the sample. The cracking of the sample is illustrated in figure 33.

Figure 34:Sample representing the crack formation in 15- and 0-degree samples

The graphs for the samples with 0 degree and the graphs for the samples with 15-degree angle and different radiuses is shown in figure 34. Samples that have 0-degree angles are plotted by the blue graphs, while samples with angle 15 and radius 10 is plotted as red graphs. Lastly the grey graph shows a sample that have 15-degree angle and 1.585 mm radius. As can be seen from the graphs the samples with 15 degree and with 10 in radius takes the most force before reaching failure. This can look a bit strange at first because they have less thickness in the middle than the samples with 0-degree angels. Therefore, one would think that the samples with 0-degree angle would be stronger. However, when taking into consideration that all these samples crack in the holes and not in the middle, the results make more sense. The variation in strength is considered to be because of test setup and density of the samples, rather than the geometry in the case of these samples. Due to the cracks appearing in the hole's further analysis of the variation in graphs are considered not to be important. The results of these tests were expected but was considered necessary to perform them in order to rule out this geometry.

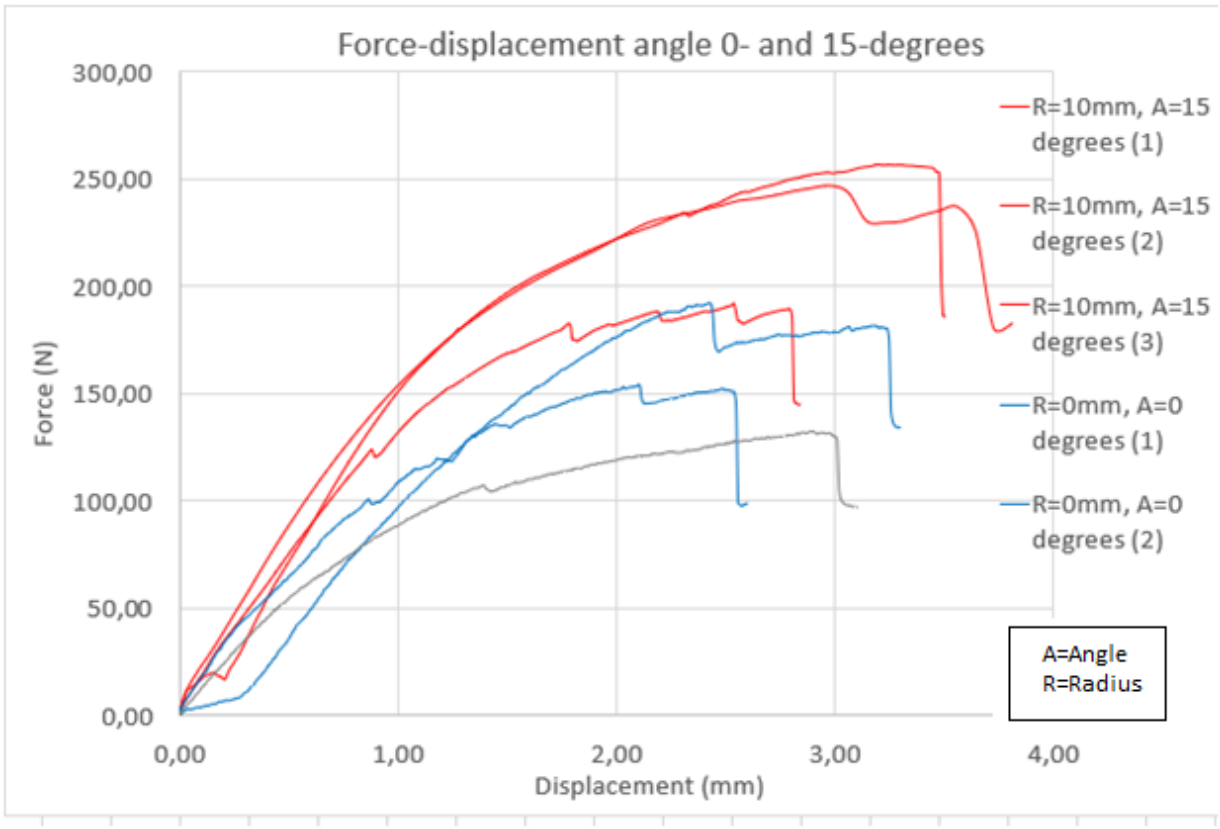

Figure 35:Graphs showing Force-displacement curves of samples with angle 0 and 15 degrees. The blue graphs show the force-displacement curve from the samples with angle 0. While the red graphs are curves from testing samples with radius=10mm and angle=15 degrees.

Samples with 45-degree angle combined with different radiuses

For the samples that were manufactured with 45 degrees different development of cracks were experienced for the different radiuses. For the sample with 0 in radius the cracks formed similarly to the original butterfly-sample with aluminium reinforcement. The crack was in the middle but moved towards one of the holes above were the crack starts. This is seen in the sample to the left in figure 35.

For the sample that had radius of 5 it cracked near the middle and the direction of the crack moved toward the hole of the sample. When increasing the radius to 10, it was discovered that the cracks started farther away from the middle and that the cracks moved towards the holes. This indicates that when the radius increases, the cracks move farther away from the middle. It is worth noting that the thickness in the middle of the sample increases with increasing radius, making it harder to crack in the middle, seen in figure 35.

Figure 36: Samples with 45-degree angle and different radiuses. To the left radius 1. In the middle radius 5. To the right radius 10

The graphs for the samples with 45-degree angle and different radiuses is shown in figure 36. The graph represents all the tests taken with samples that have 45-degree angles. In order to analyse the graphs, the results have been divided into different groups and compared.

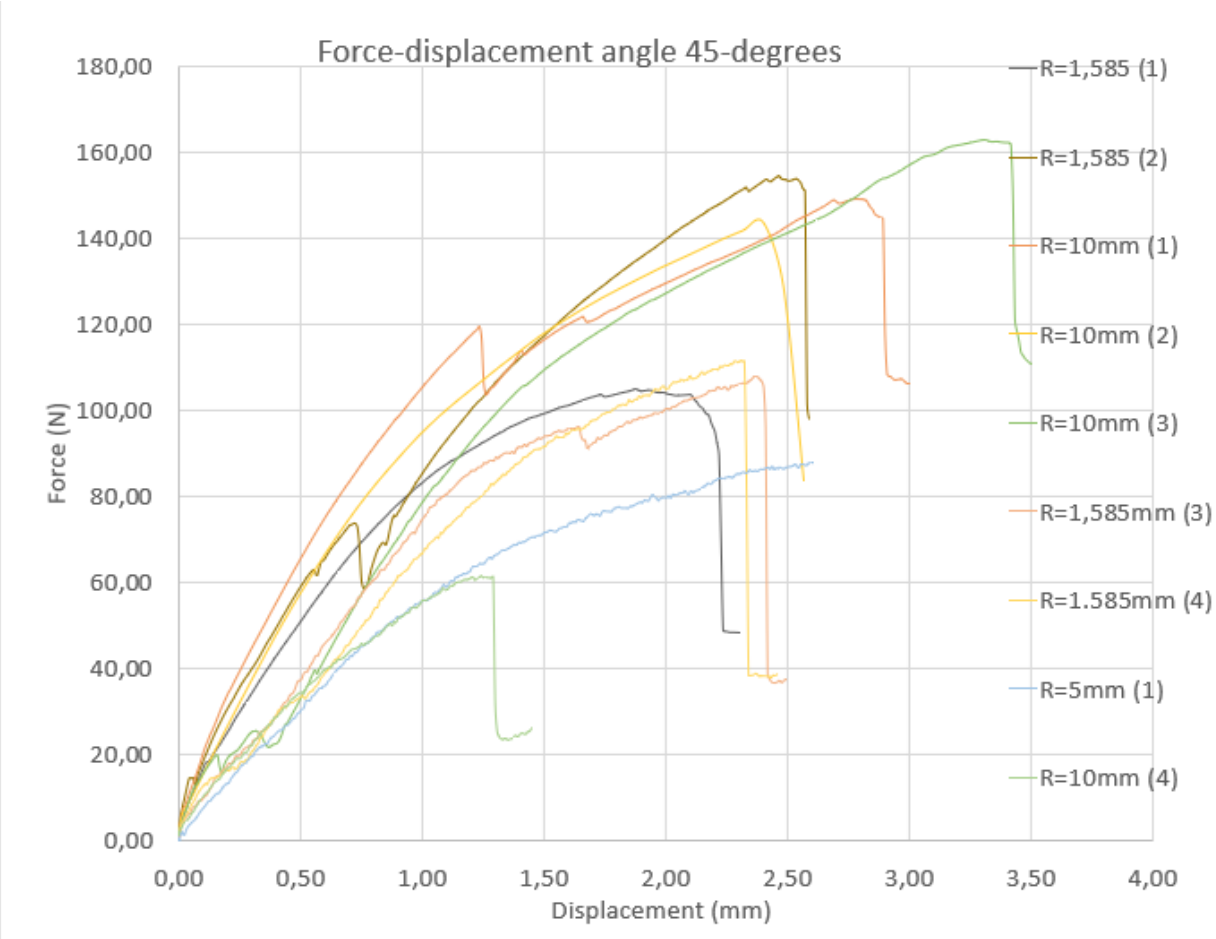

Figure 37:Force-displacement curve for samples with 45-degree angles and different radiuses.

First the curves from testing samples with 45-degree angle and 1,585 mm radius are grouped together in one graph, in figure 37. This is the butterfly sample with no change in geometry. In this graph three of the curves are similar, while one of the curves show a lot more strength than the other three curves. This difference in strength cannot be regarded as a difference in density and it is most likely due to wrong setup of the sample, and it is probably the 3d-printed plastic devices that provide extra strength to the sample.

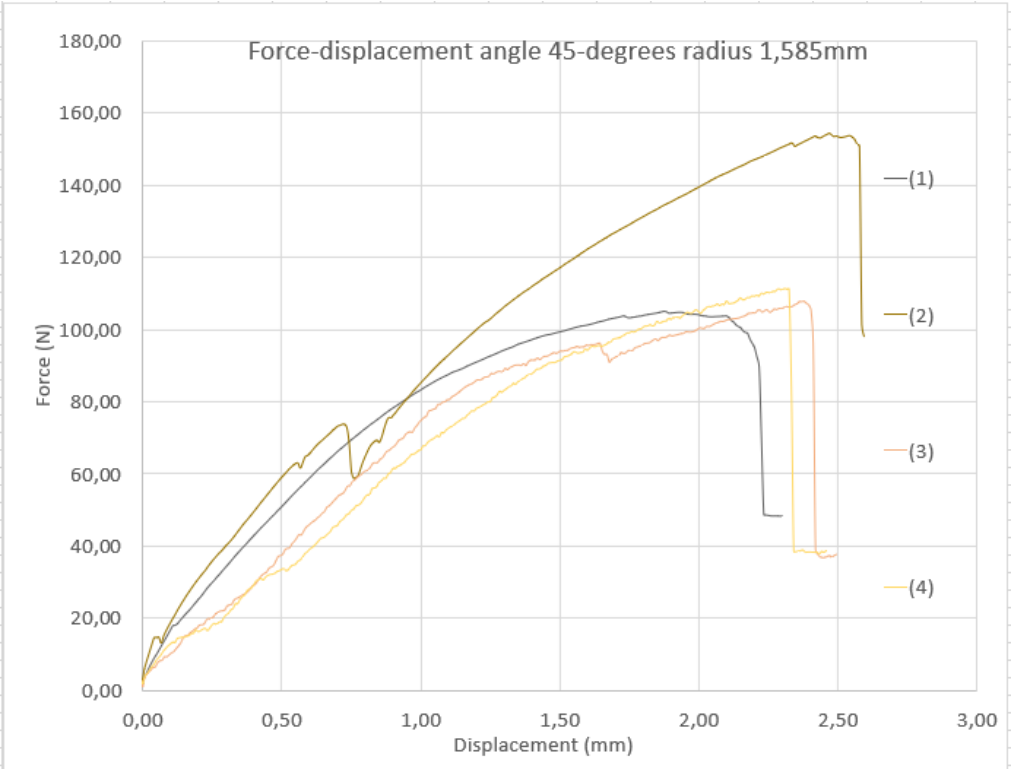

Figure 38:Force-displacement curves for samples with 45-degree angles and radius 1.585.

Then a graph was made to show the curves from the test of the samples that have 45-degree angles and 10mm radius and can be seen in figure 38. What can be seen from this graph is that the curves are mostly similar except for one graph that is much weaker than the other graphs. The reason why this curve is much weaker than the other curves is unknown, but it could be because it has received deformations when made and or handled.

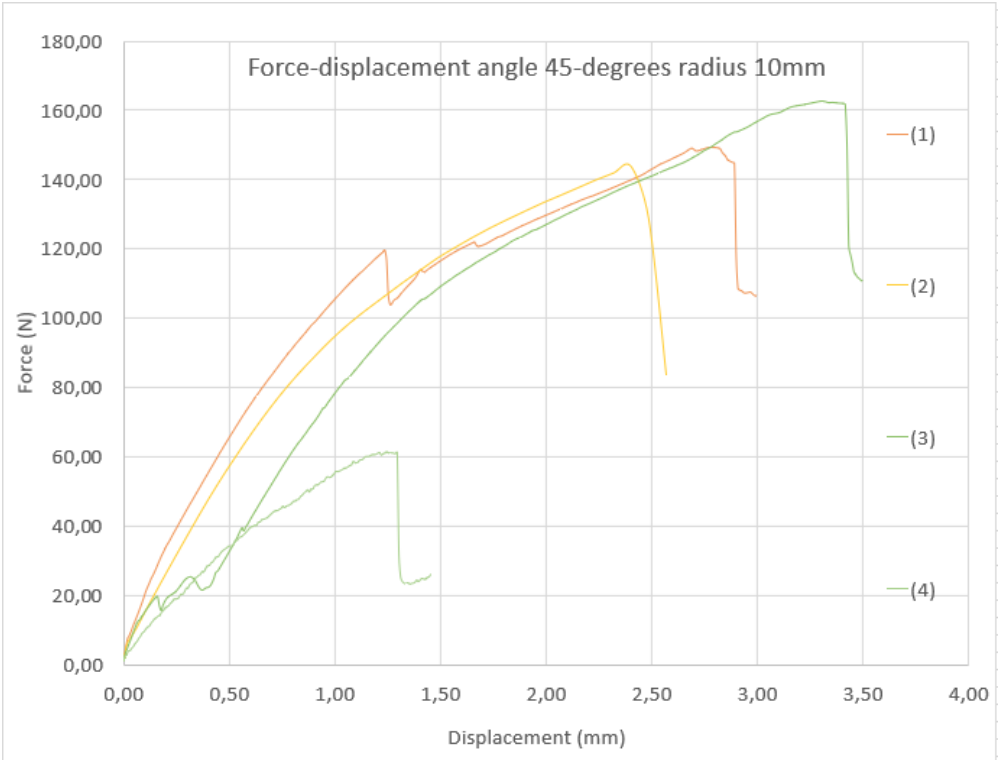

Figure 39: Force-displacement curves for samples with 45-degree angles and radius 10 mm.

In the figure 39, the force-displacement curve for a shear tested sample with radius 5mm and angle 45 degrees is showed. Due to only one test being taken with this sample it is difficult to say if it is a good representation of how the curves with this sample geometry behaves. However, in figure 40 it is compared to other curves to see whether it makes sense. The reason why only one test was performed on the sample with radius 5 mm is because it was more interesting to see the effects of a bigger change in the radius and is why the samples with 10 mm in radius is tested in a larger amount.

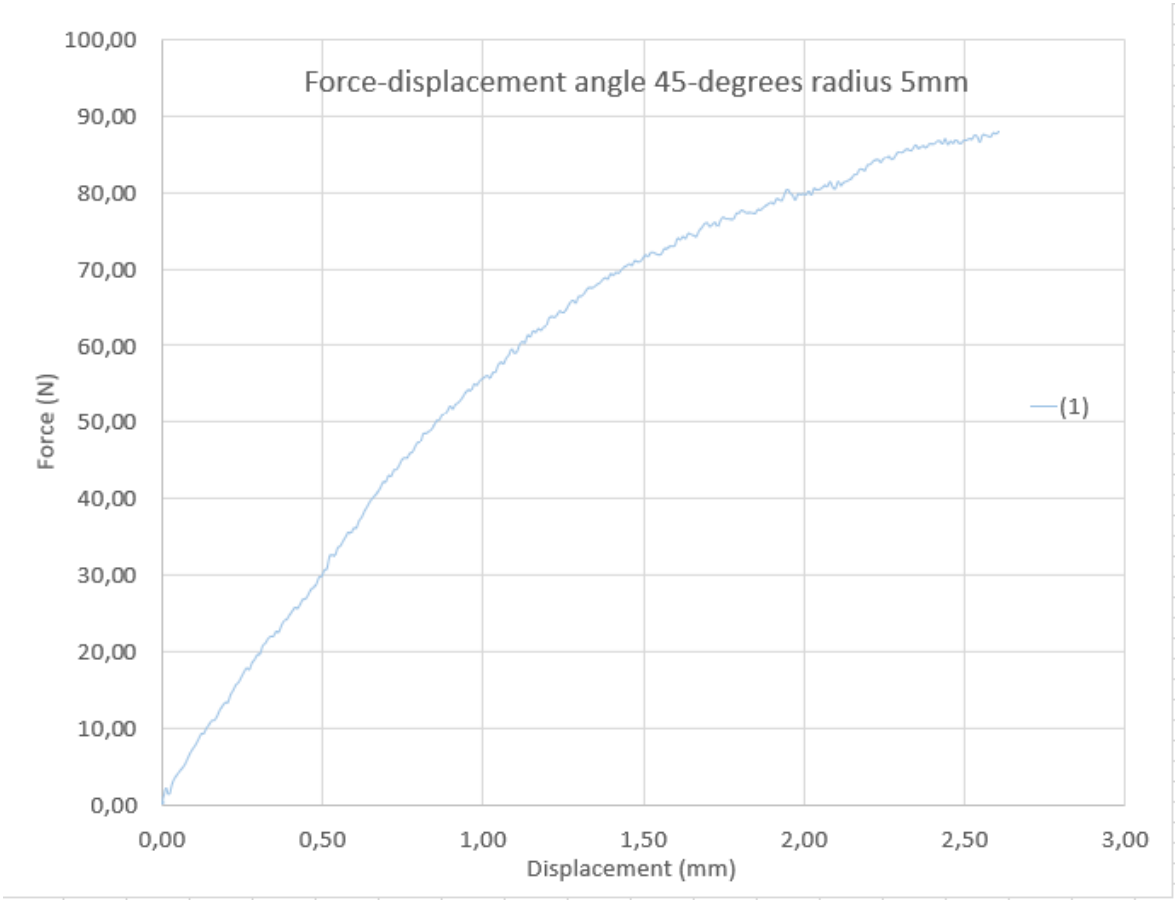

Figure 40:Force-displacement curve for samples with 45-degree angles and radius 5 mm

In figure 35 the curves with 45-degree angles and different radiuses are compared to see what the effect of the change in radius is. One representative graph is chosen for the sample with radius 10 and one representative graphs is chosen for the sample with radius 1.585. The curve showing the Force-displacement of the sample with radius 5 is the only curve obtained for this sample geometry and is not necessarily representative for the behaviour. The graphs show difference in strength where the sample with 10 mm radius is the strongest sample and the sample with radius 1.585 is the second strongest. It makes sense that the graph with 10 mm radius is the strongest because increasing radius makes the sample thicker in the middle. However, this is not the case for the curves showing the behaviour of the sample with 5 mm radius, which is weaker than the sample with 1,585 mm radius. Therefore, it is suggested that the blue graph is not representative for the behaviour of the samples with 5mm radius. To sum up, an increase in the radius makes the samples thicker in the middle is suggested as the reason for the differences in strength.

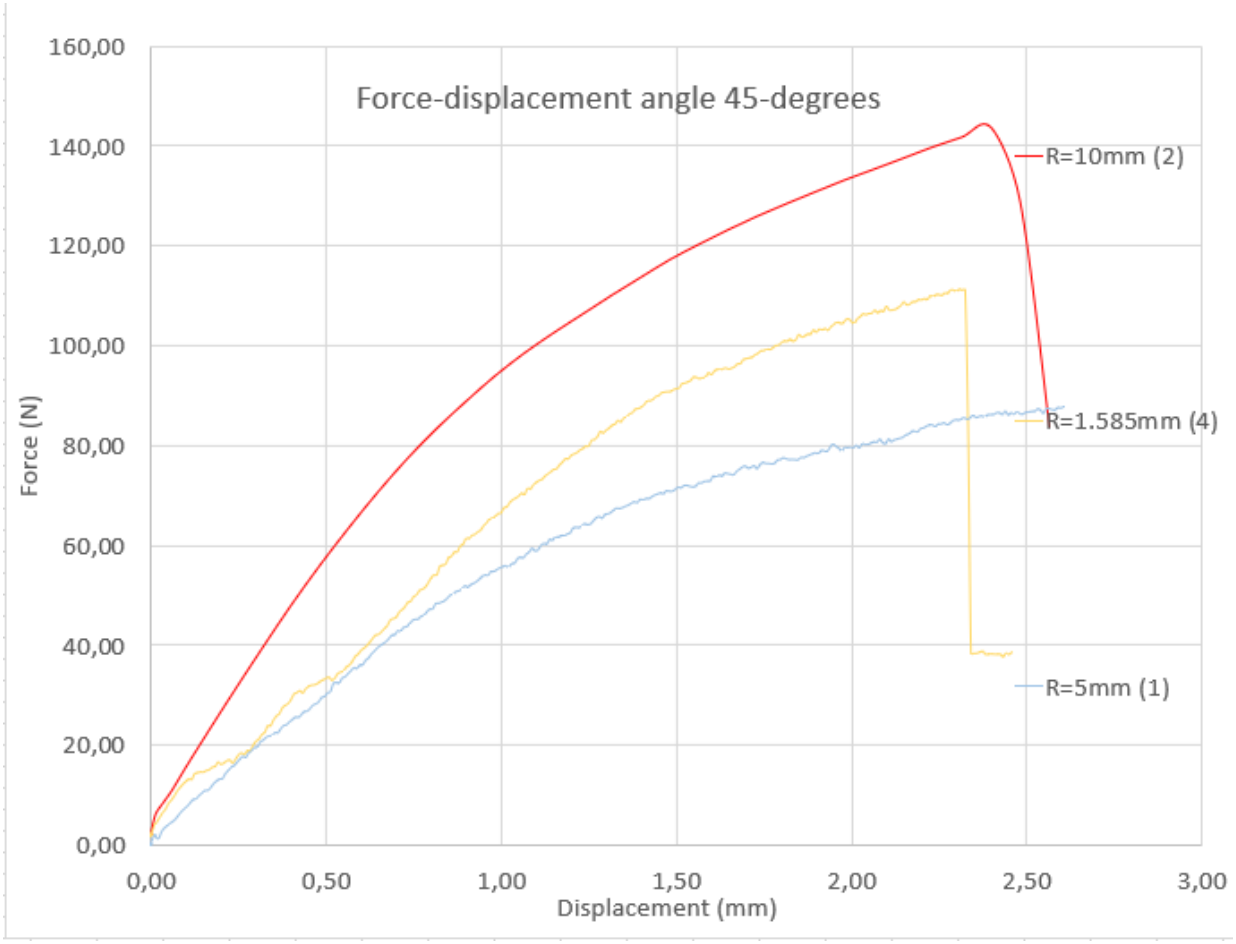

Figure 41: Representative force-displacement curves for samples with 45-degree angles and radius 1.585mm,5mm and 10mm

Samples with 50-degree angle combined with different radiuses

For the samples that were made with 50 degrees and different radiuses it was found that it was similar to the samples with 45 degrees. The crack pattern for the 50-degree sample with 0 in radius the cracks are in the middle and the direction of the crack is moving towards the hole of the samples, as seen in figure 41. The samples with 5 and 10 in radius, cracks farther from the middle with increasing radius. In these pictures the sample with 10 in radius crack closer to the middle, but it is most likely due to the setup of the sample and deformations before the test.

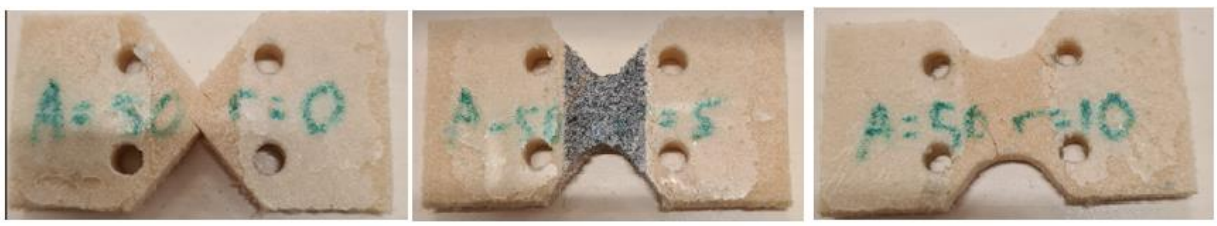

Figure 42:Samples with 50-degree angle and different radiuses. To the left: r=0. In the middle: r=5. To the right: r=10.

The graphs for the samples with a 50-degree angle and different radiuses is shown in figure 42. The curves show the same behaviour for the graphs with 45-degree angle, where the samples are stronger with larger radius. The graphs with 0-degree radius are the green and the grey curve showing similar behaviour to each other. The black curve is the sample with 1.585 in radius showing greater strength

than the samples with 0 degree and less strength than the samples with 5 mm radius. The samples with 5 mm radius are the blue and the yellow graph and are similar to each other suggesting that they are representative for the behaviour of a sample with this geometry.

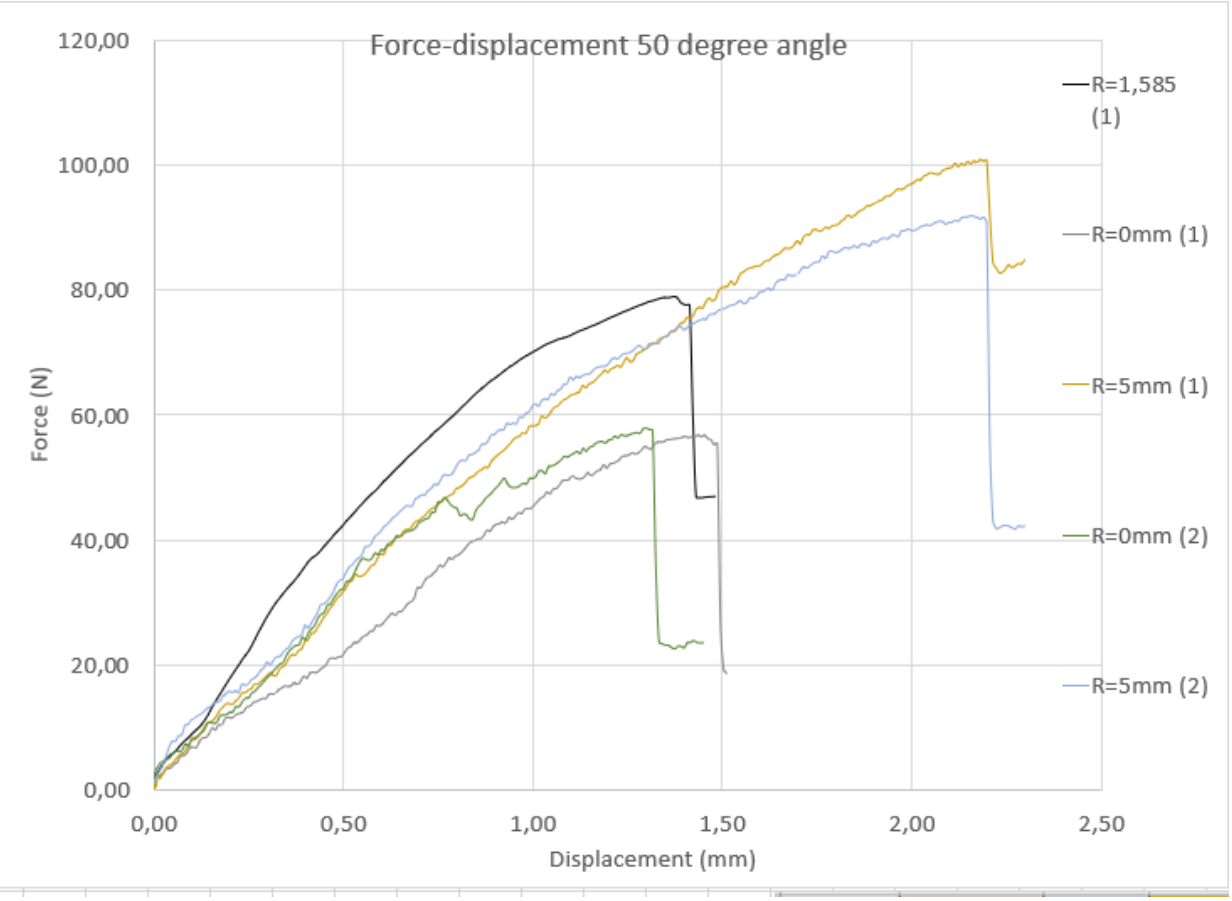

Figure 43:Force-displacement curve for samples with 50-degree angles and radiuses 0mm, 1.585mm and 5mm

To sum up, the effect of the radius of the samples is that the sample crack farther from the holes with increasing radius. In terms of strength, the samples with larger radius can receive larger deformation and withstand higher force than the samples with smaller radiuses. In addition, smaller angles of the samples result in cracking farther from the middle and higher strength of the samples. By performing these tests with different radiuses and angles it is confirmed that a different geometry does not result in pure shear. The samples with 45 degrees and 50 degrees and radiuses of 1.585mm and 0mm show the most promising formation of cracks in terms of the desired result.

3.3.3 Inaccuracies

It is important to be aware of the different inaccuracies that exist when analysing the results of the shear test. When doing the shear tests on the Divinycell foam with the setup and sample that is described, different factors affect the accuracies of the results. During the manufacturing of the sample with the CNC-machine some microscopic deformations could occur in the foam. Some imperfections in the microstructure like this could make the sample crack differently than it would with no change to the microstructure. In addition, damage to the microstructure may have occurred when the sample was

handled in the gluing process and when the sample was placed inside the two L-shapes. Before the plastic plate was added to make the L-shapes not being able to move during mounting a few samples were cracked even before the testing and some samples that were tested may have received damage that was not visible. Another inaccuracy occurred, after adding the 3d-printed plastic parts to the setup, where some samples received additional strength because the plastic part got stuck due to it being a bit too large when doing initial testing with it. This is commented on the graphs when this problematic may have occurred. Also, when placing the L-shapes in the compression machine it was difficult to make the bottom L-shape stand straight on the compression plate and some tests may have been affected by this. Lastly, some of the Divinycell was exposed to light making them a brighter yellow colour than the Divinycell was stored in the shadow, which could affect the material properties. Optimally, all of the Divinycell should be stored a dark place. However, it is not believed that the inaccuracies listed is enough to make the sample not shear in the middle during the test. The inaccuracies mentioned that could affect the crack pattern is wrong setup of the 3d-printed plastic parts and the placement of the L-shapes in the compression machine, but the crack pattern was the same even when these inaccuracies was not present. These inaccuracies are considered negligible but could create some differences in strength that is not due to the density of the material.

3.3.4 Different shear setups

Due to the challenges that came with doing shear tests on Divinycell with the current shear setup, an investigation has been made to see how other researchers have performed these tests. Generally, Divinycell is a difficult material to perform shear tests on and an optimal solution for the setup is yet to be found when looking through articles. However, shear tests that sufficiently establish the shear properties of the material is found.

In Bolf et al. they perform a shear test based on the ASTM C273 standard to get the necessary properties from the shear test.[52] They found that there is not a detailed description about how the samples are manufactured and prepared and offer a detailed description about how it can be done. By recording the tests, they could use DIC technology to calculate the shear stress and shear modulus. The article conclude that it is important to verify the material properties that is provided from the manufacturer before it is used in calculation. The setup suggested in ASTM C273 [53] has been shown to be accurate for polymeric foams and have been used successfully in other reports as well [52, 54, 55]. In this setup a prism of divinycell is glued to the walls of loading plates. Then shear test is done either by moving the loading plates against each other in compression or in tension where the loading plates move away from each other. The graphs that are made from testing the foam with this setup is discovered to be a bit inconsistence and comparisons to other articles doing the same tests are usually necessary to verify the results.

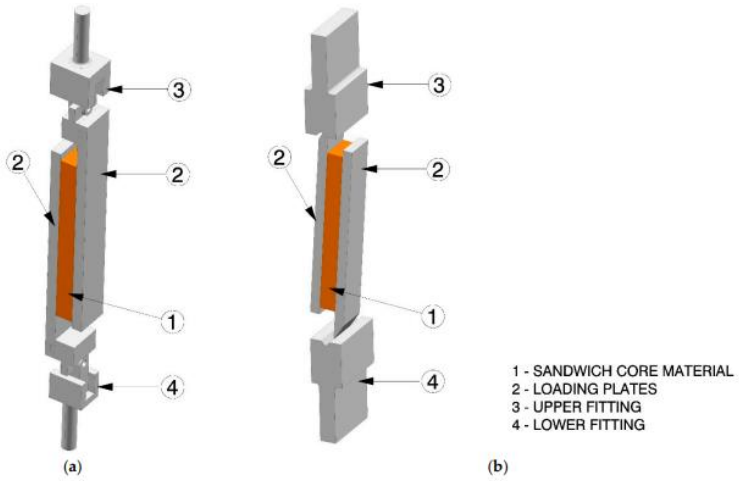

Figure 44 Shear test used for Divinycell. Picture from: [54]

In Taher et al. [56] test were performed with a with a setup that can apply tension and compression load as together with shear load. In the report the shape of the test specimen used are similar to the test sample in this thesis. The sample of the report uses the same angle, 45 degrees, as the originally described in this thesis but Taher et al uses a radius that is larger. However, due to investigation of different radiuses in this thesis a bigger radius for the samples is not better in our case.

A similar setup compared to the current study of shear tests are used in Aktas et al. [50] and described in ASTM Standard D 7078 [57, 58]. The report used two L-shapes that is dragged apart during testing. The difference between the current study and the report is that the sample is fastened in the L-shape with clamps instead of metal cylinders. In addition, the setup is loaded in tension and not compression like the current thesis. The differences in these test setups are later analysed and discussed.

4. Numerical analysis

An aim of this project study was to represent the mechanical behaviour of the PVC foam by using an existing finite element material model. Specifically, it was wished to look into the Deshpande-Fleck material model as it has proven to be a viable choice for different type of foams [28, 29]. From the experimental research done earlier the main results that are deemed viable are those from the quasi-static uniaxial compression test. Therefore, these uniaxial compression tests are to be represented by finite element modelling. Thus, in the following chapter information is presented regarding the finite element modelling of quasi-static compression results have been done, and comparison of actual test results to results acquired from the numerical analysis.

4.1 Implementation of the Deshpande-Fleck material model in LS-DYNA

The main goal of the finite element analysis (FEA) is to accurately represent the mechanical behaviour of the Divinycell H80 foam in quasi-static uniaxial compression. This being based of the viable results that were achieved during the experimental research. Therefore, a FE material model which mainly utilizes the stress-strain response of a material in compression is of interest. With this in mind, the constitutive model developed by Deshpande and Fleck implemented in LS DYNA by Reyes et al (MAT154) was chosen [5]. This is because the material model in LS DYNA mainly just needs the stress-strain curve of a given foam to represent its hardening behaviour. Though, some other parameters are also needed, they are intrinsic material values which have already been found. Other finite element packages, such as ABAQUS also gives the user the option of using the Deshpande-Fleck material model, but in this case values from hydrostatic compression tests are also required [42]. Therefore, LS-DYNA is the FE package of choice going forward.

4.1.1 Material model parameters

When modelling the behaviour of foams during different loading in a finite element program it is necessary to input parameters that describe the behaviour of the material. These material properties can be found from experimental testing. Equation 4.1 shows how the yield stress, Y, is expressed in the implemented material model in LS-dyna and what material properties needs to be found in order to define it [5].

$$Y = \sigma_P + \gamma\frac{\hat{\varepsilon}}{\varepsilon_D} + \alpha_2 \ln\left(\frac{1}{1-(\hat{\varepsilon}/\varepsilon_D)^{\beta}}\right) \tag{4.1}$$

When using the Deshpande-Fleck model the following parameters must be defined in order to get a curve that is similar to the experimental curve: σ_p, α_2, γ and β are material parameters and can be found from a curve fit of the stress-strain data from the uniaxial compression. The densification strain ε_D is determined from the density of the foam (ρ_f) and original foam material (ρ_{f0}) [5]. This can be seen in equation 4.2.

$$\varepsilon_D = -\frac{9+\alpha^2}{3\alpha^2}\ln\left(\frac{\rho_f}{\rho_{f0}}\right) \tag{4.2}$$

The parameter C_{fail} is another value that should be defined in LS-dyna and is the value of the failure strain of the foam and is used to remove failed elements during the simulation. It can be found using a tensile test for foams and looking at the strain where there is failure on the graph. If multiple tensile tests are taken the lower values for the failure strain are usually picked. In the case of this report is was not possible to perform tensile tests to obtain this parameter [5].

4.1.2 Choice of tests and curve fitting

To acquire the material model input parameters, which are needed for the Deshpande-Fleck foam model (MAT154) in LS-DYNA, stress-strain curves from the uniaxial compression tests were used. Additionally, parameters such as the Young's modulus and relative density of the foam specimens, which are also needed in the material model, were found in the experimental research part. To represent the behaviour of the foam, both in the in-plane direction and out of plane direction, two stress strain curves were analysed. Specifically, stress-strain curves from the samples 01 and 13 were used as these have been analysed in the earlier chapter 3. These samples were both loaded at the same strain rate, but in different directions. The strain rate dependency of the Divinycell foam has been discussed, but is chosen to not be investigated by FEA. Other materials models in LS-DYNA may be more suitable for investigation of the strain-rate dependency, such as the Fu-Chang's foam with rate effects model (MAT83) [35].

For the curve fitting data from the stress-strain curves were fitted to a curve described by the equation 4.1 to acquire the parameters of plateau stress σp, Υ, $\alpha 2$ and β. To do the curve fitting by the equation 4.1 the compaction strain ε_d was also needed. This value is based on the parameter describing the shape of the yield function, α, and the relative density of the foam, as seen in equation 4.2. From literature on Divinycell foam, and visual inspections of samples after the compression tests, it is known that the material displays a nearly zero plastic Poisson's ratio [28, 59]. Thus, by using equation 2.7 one gets a value for α. Once these values are known one can perform the curve-fitting, which is illustrated in figure 43. The figure 43 presents the stress-strain curves from compression tests done on samples 01 and 13, and the curve fit which was used to acquire the model parameters. The curve fit does not include de-loading, or initial elastic values, as hardening is the primary focus, and the inclusion can give inaccurate values for the model parameters. Model parameter values from the curve fitting are given in table 7 for both tests. Additionally, the value for the failure strain of the foam, C_{fail}, is found from literature and is based on the volumetric strain at failure for Divinycell H80 foam [59].

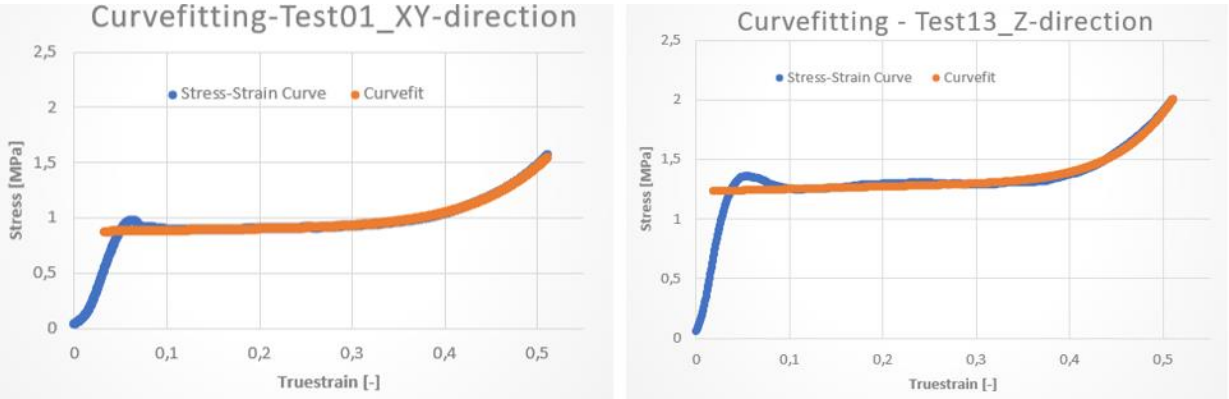

Figure 45: Showcasing of the Deshpande-Fleck yield surface curve fitting which was done for both tests 01 and 13 based on experimental data

Table 7: Input parameters for the Deshpande-Fleck foam model (MAT154) for both tests specimens 01 and 13 in LS-DYNA

Test 01									
ρ_f *[kg/m³]*	E_f *[Mpa]*	ν_p	α	Υ	ε_d	α_2	β	σ_p *[MPa]*	C_{fail} *[59]*
81,7	*23,2*	*0*	*2,12*	*0,40*	*2,84*	*4,87*10⁴*	*6,58*	*0,87*	*0,1*
Test 13									
ρ_f *[kg/m³]*	E_f *[Mpa]*	ν_p	α	Υ	ε_d	α_2	β	σ_p *[MPa]*	C_{fail} *[59]*
80,0	*36,4*	0	*2,12*	*0,59*	*2,86*	*2,18*10⁶*	*8,70*	*1,23*	*0,1*

4.2 Finite element model

The model made in LS-DYNA to represent the quasi-static behaviour of the Divinycell H80 foam is a 24x24x24 mm³ sided cube, as seen in figure 44. A solid element represents the cube, and by using the command ‘’*Shape Mesher*’’ 8000 elements were assigned to the cube. The solid elements were represented using fully integrated selectively reduced solids (*ELFORM 2*), as this has proven to be viable for foam modelling in LS-DYNA [5, 60]. To avoid hourglassing the stiffness based hourglass control (*IHQ=5*) with default values was assigned to the solid cube. Additionally, the bottom nodes of the cube are fully constrained to simulate a rigid bottom. Afterwards the Deshpande-Fleck material model (MAT154) was assigned to the cube. To replicate the behaviour of a specific sample specimen the material parameters as shown in table 7 were simply input into respective keyword files.

Next a rigid part was made by using shell elements to simulate the part of the compression machine that moves. The rigid plate was given the material properties of steel by using the rigid material model (MAT20), and a thickness of 10mm was assigned. Contact between the rigid plate and the cube is defined by using the automatic nodes to surface contact command. In this case the top nodes of the cube were made to have contact with the bottom surface of the rigid plate. Additionally, for the contact a soft based contact formulation (SOFT=1) was added. This is due to the wide difference in the elastic bulk moduli of the elements which make up the surfaces in contact, and is the preferred approach when soft foam materials interact with metals [34].

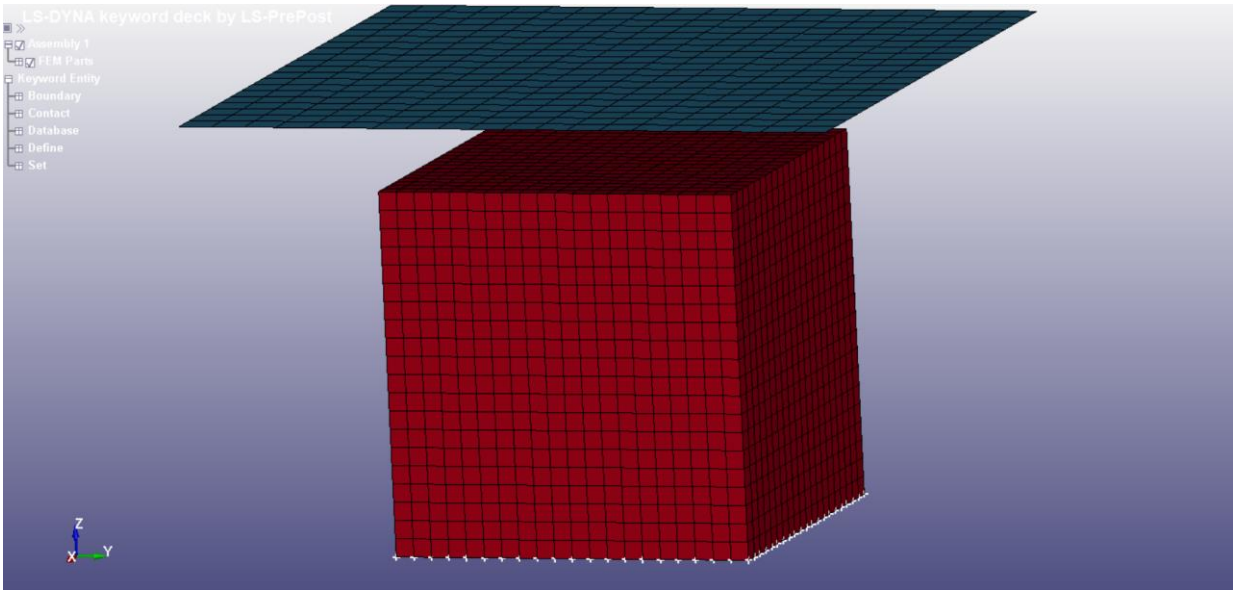

Figure 46: 24mm sided cube model made in LS-DYNA

The quasi-static loading was applied to the test cube by assigning a prescribed motion to the rigid top plate in which a velocity field was used. The shell plate was constrained so it could only move in the Z-direction, and the loading was applied by using the keyword ''PRESCRIBED_MOTION_RIGID'' with a curve defined by [5]:

$$v(t) = \frac{\pi}{\pi-2} * \frac{d_{max}}{T}\left[1 - \cos\left(\frac{\pi}{2T} * t\right)\right] \quad (4.3)$$

Here, d_{max} is the final displacement of the top plate, while T is the total loading time. The given velocity field from time t=0 to t=T, results in the displacement d_{max}, resulting in an initial acceleration which equals zero. This should ensure that the loading takes place gradually, thus needless dynamics in the numerical solutions are avoided. For the FEA the total loading time was set to 100ms, and the maximum displacement was 16mm. The 16mm displacement matching the displacement that the samples were deformed to in the experimental research part.

4.3 Finite element modelling compression results

Results obtained from the finite element analysis were compared to the behaviour of the physical uniaxial compression tests which have been performed. The aspects that were investigated were the deformation response of the FEM sample and stress-strain curve results. This was done for both the samples 01 and 13 to investigate the load direction effects. These results were then discussed regarding the suitability of the chosen Deshpande-Fleck foam model in LS-DYNA for the Divinycell material.

4.3.1 Deformation response

Analysing the deformation response of the finite element models it is seen that there are factors that are consistent with the physical tests done, but also certain results which question the methods used for the finite element modelling. From figure 45 one can observe the deformation in the finite element

models that occurred. The same deformation response was to be seen for samples 01 and 13. The figure show deformation of the cube after a time of 80ms, where the cube is in the plateau regime, and at the end time of 100ms, where densification has occurred. It is observed that in both cases there is deformation not only in the direction of the displacement, the Z-direction, but also in the Y-direction. Though, no displacement occurs in the X-direction, from looking at the effective strain. Considering that the plastic Poisson's number has been set to zero, this is inconsistent with expected results, and must be looked into. The deformation in the Z-plane though has been modelled as observed with elements being more compressed with increasing deformation.

The reason behind this deformation in the Y-direction seems to be because of an internal buckling which occurs at one side of the model, as seen in figures 46 and 47. The figures are at a time of 80ms, the plateau regime, in the models and show that the effect occurs for both specimens 01 and 13. This buckling leads to a negative volume change in one side of the cube, resulting in a higher von Mises stress on that side of the model. While on the other side of the cube a positive volume change is observed due to the buckling. Additionally, it can be observed that a higher von Mises stress exist for the sample 13 which is loaded in the out of plane direction. This being in line with what is observed in the physical experiments done. However, the difference in von Mises stress throughout the model is actually not that large when observing the von Mises values displayed in the figures 46 and 47. Here, there is a difference of about 0,150 MPa for the model 01 and 0,300 MPa for the model 13. Even so, the deformation observed is deemed to be incorrect when compared to actual deformation observed from compression experiments.

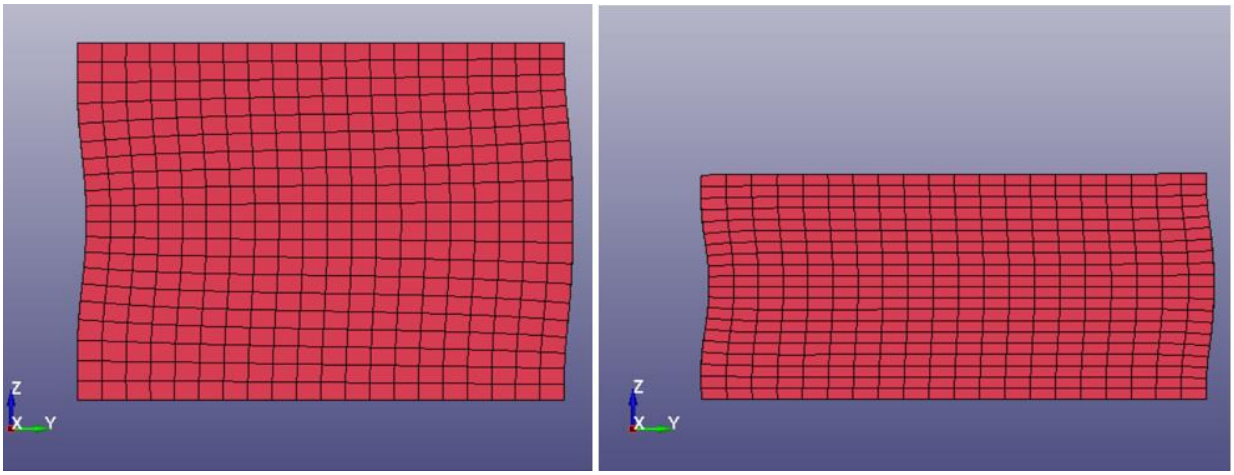

Figure 47:Deformation response of the finite element model at times 80ms and 100ms, from LS-DYNA

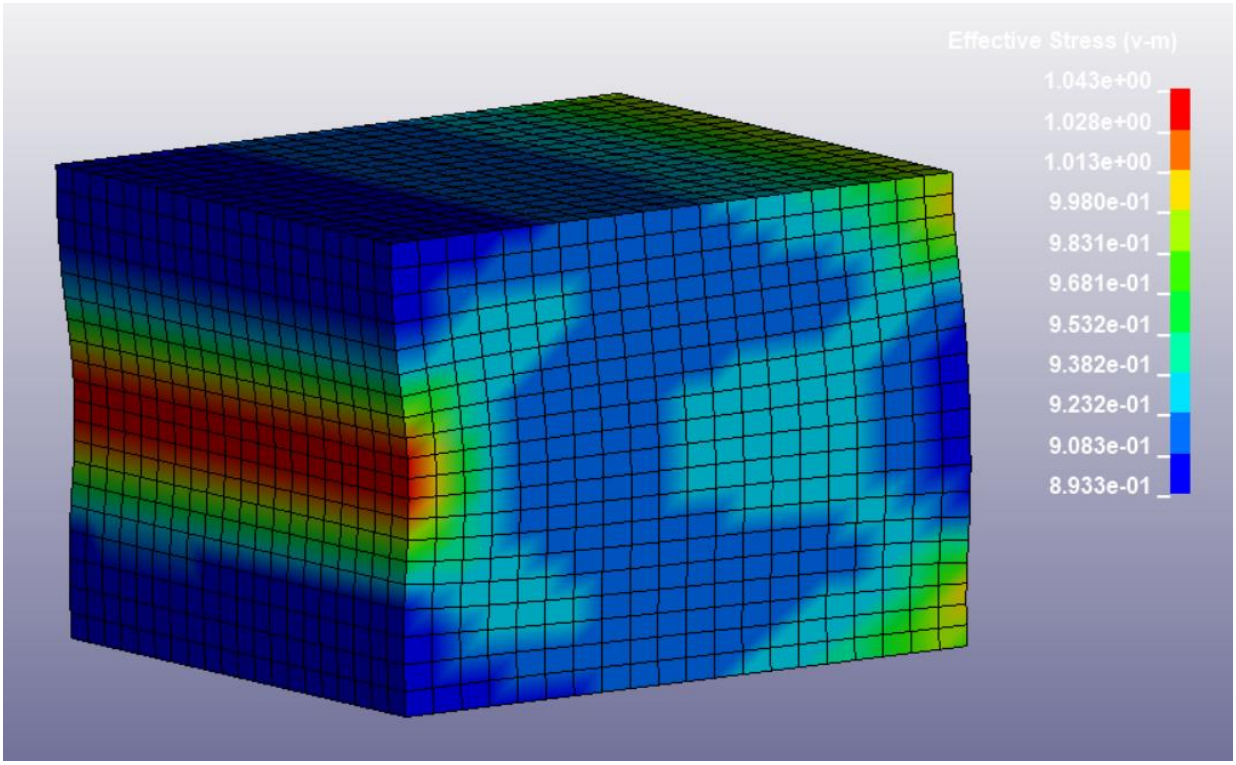

Figure 48:Finite element model based of sample 01 loaded in the in-plane direction showcasing the Von Mises stress at time 80ms, from LS-DYNA

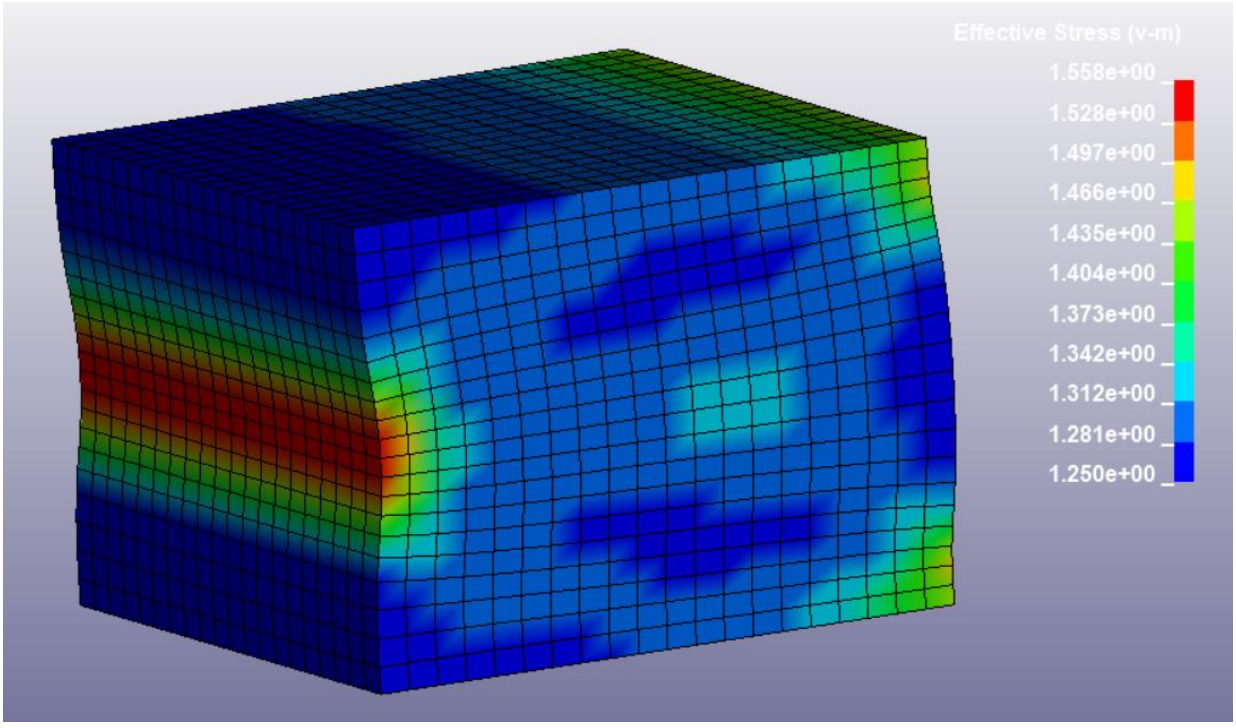

Figure 49: Finite element model based of sample 13 loaded in the out of plane direction showcasing the Von Mises stress at time 80ms, from LS-DYNA

When comparing the observed deformation with other literature work which uses the Deshpande-Fleck material model in LS-DYNA for foams this problem is not observed [5, 22, 61]. Therefore, it is assumed that some user error has been done when doing the finite element modelling. When performing a finite element analysis there are several factors which could affect the results achieved. The main cause of the error is proposed by the authors to be because of the contact formulation between the rigid plate and the cube. The large discrepancy in Young's modulus of the contact materials may have a larger effect than expected, and the contact may be more intricate to calibrate than thought. However, this is simply a theory and would have to be looked further into. Therefore, this error in deformation response must be kept in mind when looking into the viability of the Deshpande-Fleck material model in LS-DYNA when used for the Divinycell H80 foam.

4.3.2 Stress-strain curves

When looking into the stress-strain response of the finite element model in quasi-static compression these results are reasonably in line with the data from experiments. Figures 49 and 50 presents stress-strain curves for the samples 01 and 13, with respective to von Mises stress-strain curves from the FEA for comparison. The von Mises stress-strain results from the FEA are based on a set of elements which are located at the middle cross section of the cube model, as seen in figure 48. In this case all elements in the cross section are included, thus 800 elements are analysed, and an average of the von Mises stress-strain response from all the elements give the resulting curves. This is done to include the effect of the unexpected deformation in XY-plane, as the middle cross section is the most affected, and to see its effect on the results.

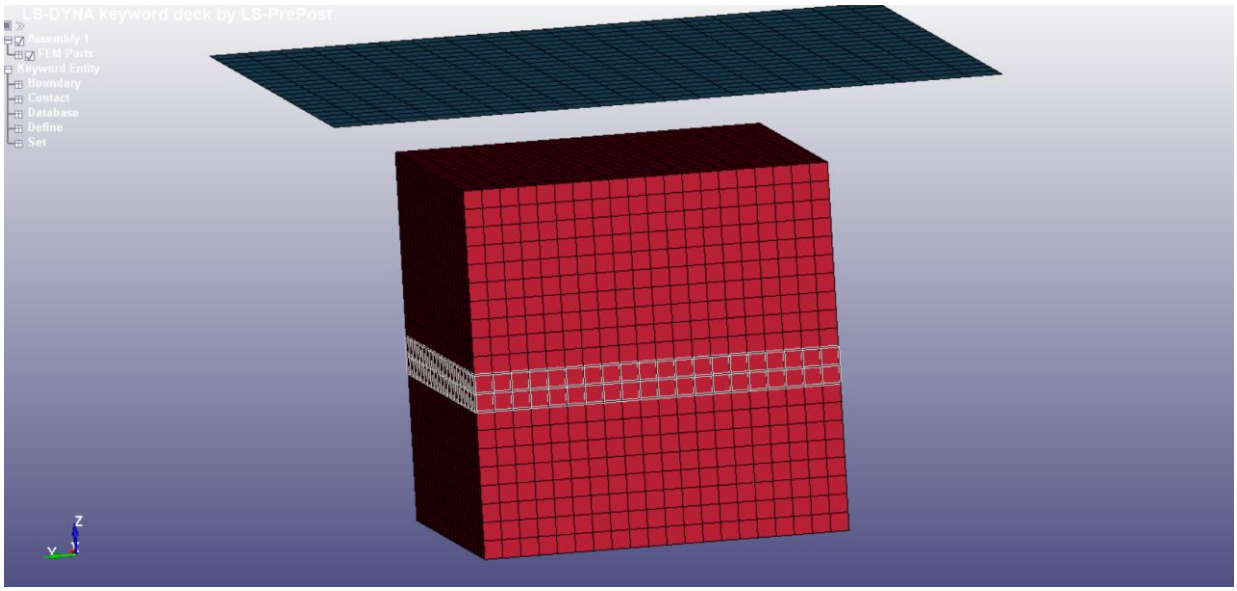

Figure 50: Finite element model highlighting the elements which were observed when looking into the stress-strain response

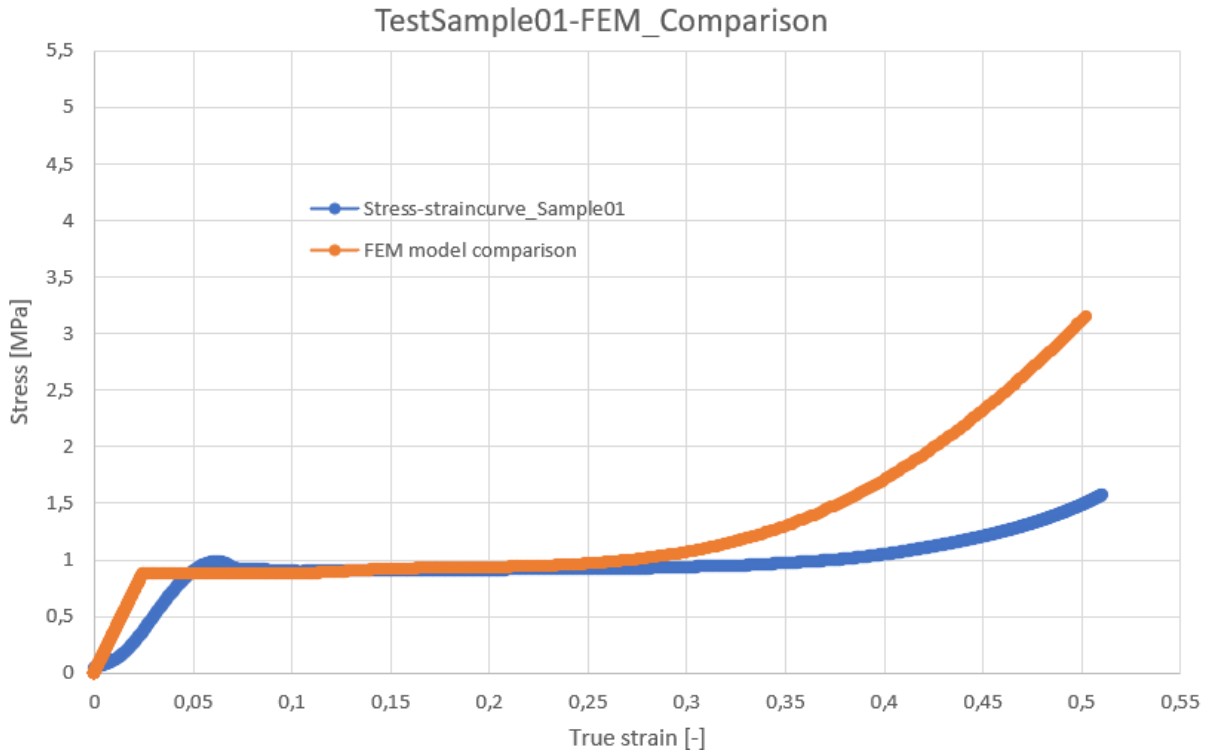

Figure 51: Stress-strain curves for the sample 01 from both experimental data and the FEM model

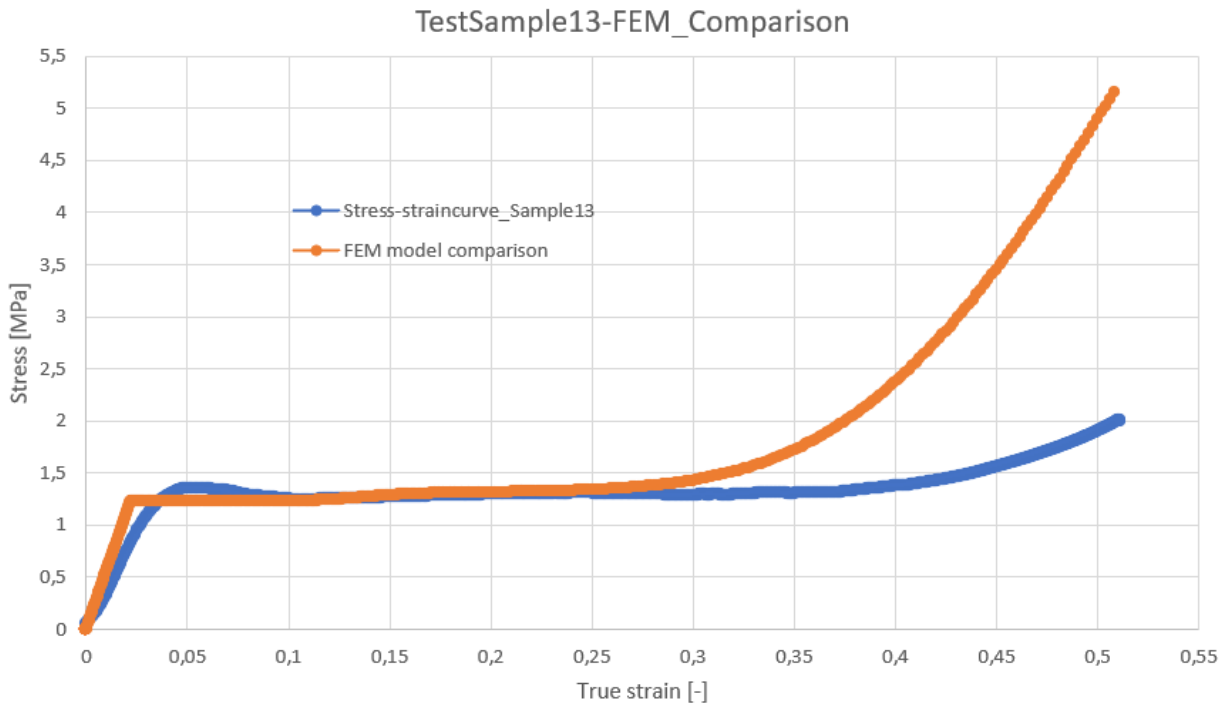

Figure 52: Stress-strain curves for the sample 13 from both experimental data and the FEM model

First, the elastic regime is investigated. For both samples it is observed that the FEA results are not perfectly accurate, though the difference is not too large. This difference in the elastic regime is due to the sample curves not instantly going into a linear response, unlike the curves from the FEM model. When comparing the linear regime of the two figures it is observed that the finite element curves are more accurate for the sample 13 loaded in the out of plane direction. This is because the out of plane loaded sample goes into a linear response quicker than the in-plane loaded sample. After the linear

regime the stress-strain curves from experiments showcase a slight peak in the stress space. This is not a response which the finite element model displays, and is deemed to be because it was not replicated in the curve fitting which was done.

Next when analysing the plateau regime, it is observed that until a certain strain the curves from the experimental data, and curves from the finite element model match. This being the case for both tests 01 and 13. However, at a strain of about 0,28 densification starts to occur for both the finite element models. Compared to the actual test data this is incorrect as seen in both figures 49 and 50, where densification occurs at a later stage. Due to this early densification the finite element curves have a much higher peak stress at the final deformation of 16 mm. The difference in peak stress is larger between experimental data and finite element results for the test 13 compared to test 01. This being because of the anisotropic behaviour of the foam where it is stronger in the out of plane direction.

There is much to look into when investigating of the accuracy of the Deshpande-Fleck foam material model in LS-DYNA in regard to the Divinycell H80 foam. Based on the stress-strain curves alone one could say that the material model with reasonable accuracy models the elastic and initial part of the plateau regime correctly. However, the densification occurs much earlier in the finite element model than in actual experimental data. It is considered that this can be due to the assumption of the density strain ε_d, which is a function of the relative density of a foam, as seen in equation 4.2. Perhaps the calibration of this density strain to the actual density strain of a material would yield more accurate results. However, it is important to note that the obtained stress-strain curves from the FEA may contain some errors due to the deformation behaviour observed. As the deformation behaviour from the FEM model does not perfectly replicate the behaviour seen from actual compression tests. This leads to speculations about how correct the finite element model was set up, and the validity of the obtained stress-strain curves.

5. Discussion

The work in this project study showcases experiments done on Divinycell H80 foam to characterize the mechanical material behaviour of the foam. From this various results have been achieved and given an insight to how the foam functions to a certain degree. Additionally, the ability to represent the behaviour of the Divinycell material by using the Deshpande-Fleck foam model in LS-DYNA was investigated, and produced results. However, these results entail some uncertainties which are to be discussed. Thus, the results from the experimental compression tests and the comparison with the finite element compression modelling is to be discussed. In addition, the shear tests results, and reasons for why they did not turn out as wished are to be discussed.

5.1 Experimental compression results and FEM compression results

5.1.1 Experimental compression results

The results which are deemed most viable from the experiments done in the project study are the uniaxial quasi-static compression results. These include investigation of strain rate, effect of load direction and effect of density variance. To confirm that these results are correct they were compared to other literature which has done the same tests [7, 47]. By doing this it was discovered that the results achieved are reasonable. However, it is acknowledged that uncertainty of the compression results exist due to possible human error and post processing of experiment data.

First, the effect of human error must be discussed, as this has the chance of occurring at many times throughout the experimental testing. Even as early as before making any samples, the 35mm thick panel which the Divinycell H80 foam samples come from can lead to errors. For example, when performing the uniaxial compression tests, it was observed that some samples had a variance in colour throughout the thickness, as seen in figure 51. This is believed to have happened due to the panel not being placed well enough so that no sunlight would hit it. Thus, this could have influenced results that have been achieved in the project study. Additionally, processes such as making samples using a CNC machine, or correct placement of samples in the compression machine, each entail a set of uncertainties which can affect the end results.

Figure 53: Divinycell H80 panel showing the variance in colour due to exposure to sunlight

Next the post processing of data achieved must be discussed, where the main outputs which were processed were the force-displacement data. When post processing data this was done in the programs Microsoft Excel and Python. Here, as seen for the calculated Young's modulus for compression tests, errors may occur. For the project study the Young's modulus was not calibrated as the results achieved were quite similar to expected results based on literature. However, it has led to some inaccurate results when analysing the stress-strain curves, and must be considered. Though, other results achieved through the post processing of the compression data are deemed quite accurate. The Divinycell H80 foam shows an anisotropic behaviour in the experiments, where it is stronger in the out of plane direction, due to the foam microstructure. Additionally, a higher density and an increase of strain rate leads to an increase in mechanical strength, the results show. These finding correspond with existing literature on Divinycell foam, thus making the viable [7, 47].

5.1.2 FEM compression results and comparison

To model the behaviour of the Divinycell foam using a finite element analysis program, LS-DYNA was chosen. As results from the compression test are the most correct experimental data, a material model which utilizes these results is needed. Thus, the Deshpande-Fleck foam model (MAT154) was chosen, as it only requires compression stress-strain data of a specimen in LS-DYNA [5]. The finite element model that was produced had the goal of replicating the compressive behaviour of cube specimen from experiments. Considering what has been done there are several aspects which can be discussed upon, and that would be beneficial to investigate further. The choice of material model for the Divinycell material, the choice of FEM program, and uncertainties of the model made in LS-DYNA could be investigated.

There are several material models which exist in LS-DYNA for foams, and that may be suitable for modelling a polymer foam. Examples of these the Low-density urethane foam model (MAT57), and the Fu-Chang's foam with rate effects model (MAT83) [34]. Using another material model in LS-DYNA, and comparing it to the Deshpande-Fleck foam model in regard to compression experiments would be insightful. By using these different material models for the same finite element model, one could see the accuracies of the different ones. Next, it would be interesting to do the compression finite element analysis in another FEM program which utilizes the Deshpande-Fleck model. For example, Abaqus which has the Crushable Foam model which is based on the Deshpande-Fleck constitutive model [42]. By doing this the results from the different FEM programs could be compared to see which is the most suitable for the material.

Finally, uncertainties in the model made in LS-DYNA must be discussed. The model which was analysed expressed reasonably viable results for the stress-strain curves when compared to the actual tests. However, the deformation behaviour of the model was not as observed in compression experiments. This is considered to be because of the contact formulation between the foam and the rigid plate acting

on it, though it must be investigated further. The inaccuracy of the deformation behaviour leads to uncertainties in the compression stress-strain graphs which were output from the FEM model. Thus, they must be viewed critically when looking into the suitability of the Deshpande-Fleck foam material model in regard to compression of the Divinycell material. Though, if the effects of this is small, the results achieved when using the material model are deemed as reasonably accurate, with an error regarding the densification strain.

5.2 Shear test results

Although the shear tests are regarded as unsuccessful it became a large portion of the thesis due to the work and time put into the test and due to a wish to analyse what went wrong during the tests and what could be changed to make the current setup work. The reason why the samples crack in the way that they do during the shear tests is still unknown, but different theories as of why have been established. The main reason is believed to be because of the nature of the microstructure of the foam. Divinycell consists of pores that are elliptic in one direction and round in two directions, making it transversely isotropic. Either because the foam is transversely isotropic or because it consists of pores or a combination of both is considered to be the reason for the observed crack pattern. In a foam the distribution of the cells is irregular, meaning that the shape of the cells are different from each other [49]. This makes the foam have locally different mechanical properties and cracks toward the part of the foams where the cells are weaker. When the foams are studied in a microscope during yielding it is discovered that deformations happen in the weakest layer of the cells of the sample. The yielded cell disrupts the formation of cells that are near the localized deformation. This disruption of cells can make the material stronger or weaker around the yielded cell. This is assumed to be a possible reason why it is hard to get the samples to shear purely. In the case of this thesis the yielding would start in the cells in the middle, but that could cause a rearrangement of the cells around this yield point making the sample crack toward the arrangement of cells that become weaker.

The graphs obtained from the testing are analysed in terms of force and displacement to see the effect of the different changes made to the test sample and the test setup. They are not analysed thoroughly because it is not considered to be important when the sample did not experience pure shear. The main takeaway from the graphs is to confirm that the changes done to the tests made sense in terms of the strength of the curves produces in a force-displacement space and to look at the consistency of the results.

When observing the images of the tests it seemed like the cells contracted at one side of the sample and that the cells moved apart from each other. This results in the side of the sample with cells moving apart being weaker than the side where the cells are closer together and after enough loading the sample crack towards the weaker side of the sample. A reason why one side gets stronger than the other could

be because only one side of the sample is moving during the tests. This could be solved by applying the same force downwards on the top L-shape as the force upward on the bottom L-shape.

The main reason for why the describes setup for the shear test was used in this thesis is because of the simplicity of the test and that modifications to the test was easily performed. By looking at the collection of the different graphs and the crack pattern for the different samples it is found that the samples with aluminium reinforced holes and angles of 45 or 50 degrees and a radius of 0 or 1,585 is considered to be the most successful tests. Reducing the thickness in the middle of these samples makes the samples weaker, but the cracks propagate in the same way.

It is believed that the test setup used in Aktas et al. [50] is more easily performed than the setup in the current study when testing pure shear of Divinycell foam. Instead of fastening the sample with metal cylinders in the L-shape they use clamps. This avoids the problem that in seen in the current thesis as the holes are weak and deform during tests. Even with aluminium reinforcement of the holes small deformations is believed to have happened in the holes during the tests. However, there might exist some challenges regarding fastening the sample with clamps that is unknows to us. If the samples are fastened by clamping the material deformation may occur due to the force that is required by the clamps to sufficiently fasten the foam. In addition, in the report of Aktas et al. the L-shapes are dragged apart, and both of the L-shapes are moving at the same speed at the same time. This is considered to be better than only loading one side at a time in compression. Whether the sample is tested in compression or tension is regarded as being not too important for achieving pure shear of the foam. However, there is reason to believe that dragging the L-shapes apart or compressing both L-shapes together at the same time is better than only one side being loaded. This is because only loading one side of the system is believed to create an imbalance that may create a small rotation and the effect of this could make one side of the sample cells stretch while the other side of the sample contracts, as is shown earlier. This ultimately results in the cracking that is observed throughout the current thesis. If the goal of the researcher is to obtain the shear properties of Divinycell another test setup is recommended to use as described in ASTM C273 standard as this test is successfully performed on Divinycell and other PVC-based foam material by reading different articles. When using this test, it is important to be aware of the accuracy of the graphs that is produced during the test and compare them with other articles to make sure the results are reasonable.

6. Conclusion

The project study has had the goal of investigating the mechanical behaviour of Divinycell H80 foam, and to represent it using an existing material model. This has been achieved to a certain extent, where viable uniaxial compression test result data was achieved. The test data showed that the Divinycell H80 foam showed an anisotropic behaviour in the experiments, where it was stronger in the out of plane direction, because of the foam microstructure. In addition, an increase in density and an increase of strain rate leads to an increase in mechanical strength. Next, the viability of an existing material model, the Deshpande-Fleck material model, in LS-DYNA was investigated in regard to the compression data. By comparing the displacement behaviour of Divinycell specimens, and stress-strain curves from experimental data to results, it was shown that results achieved when using the material model are deemed as reasonably accurate, with an error regarding the densification strain. However due to the deformation behaviour of the FEM model which was one must consider inaccuracy of these results.

Another great focus of the thesis was to determine the mechanical behaviour of the foam through shear testing on the PVC-based foam material Divinycell. As a result of the trial and failure of shear tests a greater knowledge of nature of the material was gained. The process of modifying the current test setup and test sample is explained, and some conclusion can be drawn looking at the results. First the holes of the original sample are the weakest part when tested in the current setup. Therefore, aluminium reinforcement is considered as a good addition when doing the tests with the current setup. During the initial test the distance between the L-shape became smaller and 3d-printed devices was manufactured to keep the same distance for the duration of the test and is regarded as a good addition to the test. Furthermore, a plastic plate was added to avoid deformation when the sample was handled before mounting it in the compression machine. It is concluded that less deformations happen after this was added to the testing process. Next, the graphs in the current thesis that is not accurate enough to be used for an accurate description of the mechanical properties from the shear tests. However, the graphs produced in the current thesis is mainly used for analysing the differences strength and looking at the consistency of the graph when modifications to the samples were made. The reasons why the sample did not go through pure shear is concluded to be because of the structure of the foam and due to the shear setup. Different shear setups have achieved pure shear for their samples where the shear test based on the ASTM C273 standard is regarded as the easiest test setup in order to achieve accurate result. It is also concluded that it would be better if the shear sample would be fastened by clamps instead of making holes in the sample and fastening it with cylinder, as is the case for the test described in ASTM Standard D 7078. In this test setup both the L-shapes away from each other during the test. This is considered to create less imbalance during the tests and avoid any rotation that may occur.

7. Future work

Considering future work which can be done there is a plethora to choose from. First of all, it would be very interesting to do more research on the shear test setup, and to model a finite element model to replicate the behaviour. This could give insight into why the shear tests did not go as planned. Additionally, considering the Deshpande-Fleck material model, it would be interesting to investigate the advantages of using the model in different FEM programs. One could also utilize different foam material models to observe the impact of this.

Additionally, future research could do the experiment on foams that are isotropic to see how mich it matters that Divinycell is transversely isotropic. If researchers are to do shear tests with the same kind of setup as in this thesis, they can start with reinforcing the holes of the samples with aluminium as this is regarded as a successful step towards making the samples go through pure shear. Also, the 3d-printed plastic parts, and the plastic plate made by the CNC are a helpful addition to the test. Otherwise, this research adds to the knowledge about what modifications to the test that is necessary to do and what modifications can be ruled out for future research.

it would be interesting to see how the transversely isotropic microstructure behaves under loading with the current shear test setup to see what happens to the cells on a microscopic level to it to further understand what the happens. Furthermore, for future research it is easier to use the shear setup based on the standard ASTM C273. This is because more research has been conducted with this shear setup and because good results have been achieved when compared to each other. However, if using the shear test performed in this thesis it would be interesting to see the effect of the L-shapes moving away from each other in tension, rather than only one L-shape moving in compression. In addition, changing the way the sample is fastened from being fastened with cylinders in holes of the sample to a fastening system that uses clamps could be looked into further.

References

1. Tomin, M. and A. Kmetty, *Polymer foams as advanced energy absorbing materials for sports applications—A review.* Applied plymer science, 2021. **139**(9).
2. *Gibson, L., & Ashby, M. (1997). Cellular Solids: Structure and Properties (2nd ed., Cambridge Solid State Science Series). Cambridge: Cambridge University Press. doi:10.1017/CBO9781139878326.*
3. *Reyes, A., & Børvik, T. (2018). Quasi-static behaviour of crash components with steel skins and polymer foam cores. Materials Today Communications, 17, 541-553.*
4. Maheo, L., et al., *Multiaxial behavior of foams - Experiments and modeling*. Vol. 94. 2015.
5. *Reyes, A., Hopperstad, O.S., Berstad, T., Hanssen, A.G. and Langseth, M., "Constitutive modeling of aluminum*

foam including fracture and statistical variation of density", p815-835, European Journal of Mechanics

A/Solids 22 (6) (2003).

6. V.S. Deshpande, N.A.F., *Isotropic constitutive models for metallic*

foams. Journal of the Mechanics and Physics of Solids, 2000. **48**: p. 1253-1283.

7. *DIAB Literature - Manuals. Technical Manual: Divinycell H.*
8. *Mills, N. J. (2007). Chapter 1–Introduction to polymer foam microstructure. Polymer Foams Handbook: Engineering and Biomechanics Application and Design Guide,, 1-18.*
9. *Wang, J., & Rai, R. (2016, August). Classification of bio-inspired periodic cubic cellular materials based on compressive deformation behaviors of 3d printed parts and fe simulations. In International Design Engineering Technical Conferences and Computers and Information in Engineering Conference (Vol. 50190, p. V007T06A003). American Society of Mechanical Engineers.*
10. *Srivastava, V., & Srivastava, R. (2014). On the polymeric foams: modeling and properties. Journal of materials science, 49(7), 2681-2692.*

11. *Hössinger-Kalteis, A., Reiter, M., Jerabek, M., & Major, Z. (2021). Overview and comparison of modelling methods for foams. Journal of Cellular Plastics, 57(6), 951-1001.*
12. *Gibson, L. J., & Ashby, M. F. (1982). The Mechanics of Three-Dimensional Cellular Materials. Proceedings of the Royal Society of London. Series A, Mathematical and Physical Sciences, 382(1782), 43–59. http://www.jstor.org/stable/2397268.*
13. *Zhu, H. X., Knott, J. F., & Mills, N. J. (1997). Analysis of the elastic properties of open-cell foams with tetrakaidecahedral cells. Journal of the Mechanics and Physics of Solids, 45(3), 319-343.*
14. *Chen, L. (2012). Developing constitutive equations for polymer foams under cyclic loading. The University of Akron.*
15. *Zenkert, D., & Burman, M. (2009). Tension, compression and shear fatigue of a closed cell polymer foam. Composites Science and Technology, 69(6), 785-792.*
16. Motz, C. and R. Pippan, *Fracture Behaviour and Fracture Toughness of Ductile Closed-Cell Metallic Foams.* Acta Materialia, 2002. **50**: p. 2013-2033.
17. *Diab. Divinycell – PVC materials with excellent strength-to weight. (n.d); Available from: https://www.diabgroup.com/products/divinycell-pvc/.*
18. *jamestowndistributors. Divinycell Plain Sheet. (n.d); Available from: https://www.jamestowndistributors.com/product/product-detail/1588.*
19. Westbye, E. and M. Yosufzai, *Theoretical background and numerical analysis of microcellular materials - A project report by the current authors.* 2021: p. 27.
20. Berg, R. and A. Billberg, *Modelling the mechanical response of cellular PVC*

foams using detailed finite element analysis, in *Department of Industrial and Materials Science*. 2019, Chalmers University of Technology: Goteborg, Sweden.
21. *Chen, L., & Fatt, M. S. H. (2013). Transversely isotropic mechanical properties of PVC foam under cyclic loading. Journal of Materials Science, 48(19), 6786+. https://link.gale.com/apps/doc/A345073387/AONE?u=googlescholar&sid=googleScholar&xid=da7ebe70.*

22. *Júnior, Mauricio & Soares, Gustavo & Angélico, Ricardo & Canto, Rodrigo & Tita, Volnei. (2012). Study of an Anisotropic Polymeric Cellular Material Under Compression Loading. Materials Research. 15. 359-364. .*
23. *Brekken, K.A., et al., Sandwich Panels with Polymeric Foam Cores Exposed to Blast Loading: An Experimental and Numerical Investigation. applied sciences mdpi, 2020. 1: p. 36.*
24. *Wahl, L., S. Maas, and D. Waldmann, Shear Stresses in Honeycomb Sandwich Plates: Analytical Solution, FEM and Experimental Verification. SAGE Publications, 2011. 4.*
25. *Maconachie, T., Leary, M., Lozanovski, B., Zhang, X., Qian, M., Faruque, O., & Brandt, M. (2019). SLM lattice structures: Properties, performance, applications and challenges. Materials & Design, 183, 108137.*
26. *Saint-Michel, F., Chazeau, L., Cavaillé, J. Y., & Chabert, E. (2006). Mechanical properties of high density polyurethane foams: I. Effect of the density. Composites Science and Technology, 66(15), 2700-2708.*
27. *Goods, S. H., Neuschwanger, C. L., Whinnery, L. L., & Nix, W. D. (1999). Mechanical properties of a particle-strengthened polyurethane foam. Journal of Applied Polymer Science, 74(11), 2724-2736.*
28. Deshpande, V.S. and N.A. Fleck, *Multi-axial yield behaviour of polymer foams.* Acta Materialia, 2001. **49**(10): p. 1859-1866.
29. *Deshpande, V.S. and Fleck, N.A., "Isotropic models for metallic foams", p1253-1283, Journal of the Mechanics and*

Physics of Solids 48 (2000).
30. Carranza, I., et al., *Characterising and modelling the mechanical behaviour of polymeric foams under complex loading.* Journal of Materials Science, 2019. **54**(16): p. 11328-11344.
31. Peng, Q., et al., *Dynamic Impact of High-Density Aluminum Foam.* Acta Mechanica Solida Sinica, 2022. **35**(2): p. 198-214.
32. *Kim, N. H. (2014). Introduction to nonlinear finite element analysis. Springer Science & Business Media.*
33. *ABAQUS 6.14 Documentation. Dassault Systemes Simulia Corp. Providence, RI, USA, 2014.*
34. *LS-DYNA®Keyword User's Manual Volume II, R11.0. Livermore Software Technology Corporation (LSTC). Livermore, Ca., USA, 2018.*

35. *Croop, B., Lobo, H., & DatapointLabs, N. Y. (2009, May). Selecting material models for the simulation of foams in LS-DYNA. In 7th European LS-Dyna Conference (pp. 1-6).*
36. *Ozturk, U. E., & Anlas, G. (2011). Finite element analysis of expanded polystyrene foam under multiple compressive loading and unloading. Materials & Design, 32(2), 773-780.*
37. *Perillo, M., Primavera, V., Carofalo, A., De Giorgi, M., & Nobile, R. (2010, June). Validation of material models for the numerical simulation of aluminum foams. In 11th International LS-DYNA® Users Conference.*
38. *Fang, H., Bi, J., Zhang, C., Gutowski, M., Palta, E., & Wang, Q. (2017). A constitutive model of aluminum foam for crash simulations. International Journal of Non-Linear Mechanics, 90, 124-136.*
39. *Dassault Systemes. Abaqus Analysis User's Guide, 6.14 edition, 2014.*
40. *Dassault Systemes. Abaqus Analysis User's Guide, 6.14 edition, 2014. Retrieved from 22.5.2*

Hyperelastic behavior in elastomeric foams.
41. *Dassault Systemes. Abaqus Analysis User's Guide, 6.14 edition, 2014. Retrieved from 22.9.1 Low-density foams.*
42. *Dassault Systemes. Abaqus Analysis User's Guide, 6.14 edition, 2014. Retrieved from 23.3.5 Crushable foam plasticity models.*
43. *WHAT IS CNC MACHINING? 6 OF THE MOST COMMON CNC MACHINES*. 2020; Available from: https://www.uti.edu/blog/cnc/6-cnc-machines.
44. JOHN. *Shapeoko 4 CNC Review [2022]- The Good and Bad*. 2022 JANUARY 08, 2022; Available from: https://mellowpine.com/cnc/shapeoko-4-cnc-review/.
45. Abdulqader, A. and D.C. Rizos, *Advantages of using digital image correlation techniques in uniaxial compression tests.* Results in Engineering, 2020. **6**: p. 100109.
46. *Saenz, E. E., Carlsson, L. A., & Karlsson, A. (2011). Characterization of fracture toughness (G c) of PVC and PES foams. Journal of materials science, 46(9), 3207-3215.*
47. *Saeid, A. A., & Donaldson, S. L. (2016). Experimental and finite element evaluations of debonding in composite sandwich structure with core thickness variations. Advances in Mechanical Engineering, 8(9), 1687814016667418. .*

48. *Tita, V., & Caliri Júnior, M. F. (2012). Numerical simulation of anisotropic polymeric foams. Latin American Journal of Solids and Structures, 9(2), 1-21. .*
49. Tang, Y., et al., *Experimental investigations on phenomenological constitutive model of closed-cell PVC foam considering the effects of density, strain rate and anisotropy.* Composites Part B: Engineering, 2022. **238**: p. 109885.
50. Aktaş, M. and M. Emin, *Determination of In-Plane Shear Properties of Composite Laminates.* 2022.
51. Funari, M., et al., *On the elastic and mixed-mode fracture properties of PVC foam.* Theoretical and Applied Fracture Mechanics, 2021. **112**: p. 102924.
52. *Bolf, D., Zamarin, A., Krolo, P., & Hadjina, M. (2022). Experimental Evaluation of Shear Properties of Lightweight PVC Core for Marine Application Using Digital Image Correlation System. Journal of Marine Science and Engineering, 10(2), 280. MDPI AG. Retrieved from http://dx.doi.org/10.3390/jmse10020280.*
53. *ASTM C273 Sandwich Core Shear Testing*. Available from: https://www.admet.com/testing-applications/testing-standards/astm-c273-sandwich-core-shear-testing/.
54. Bolf, D., et al., *Experimental Evaluation of Shear Properties of Lightweight PVC Core for Marine Application Using Digital Image Correlation System.* Journal of Marine Science and Engineering, 2022. **10**(2): p. 280.
55. Mostafa, A., K. Shankar, and E.V. Morozov, *In-plane shear behaviour of composite sandwich panel incorporated with shear keys methodology at different orientations: finite element study.* Journal of Composite Materials, 2013. **48**(24): p. 2945-2959.
56. Taher, S.T., O.T. Thomsen, and J.M. Dulieu-Barton. *Bidirectional Thermo-Mechanical Properties of Foam Core Materials Using DIC*. in *Thermomechanics and Infra-Red Imaging, Volume 7*. 2011. New York, NY: Springer New York.
57. *V-Notch Rail Shear test (ASTM D 7078-05)*. 2009; Available from: https://www.compositesworld.com/articles/v-notch-rail-shear-test-astm-d-7078-05.
58. *ASTM Standard D 7078-05, "Shear Properties of Composite Materials by the V-Notched Rail Shear Method," American Society for Testing and Materials, W. Conshohocken, Pa., (first issued in 2005).*

59. *Rajaneesh, A., Sridhar, I., & Rajendran, S. (2014). Relative performance of metal and polymeric foam sandwich plates under low velocity impact. International Journal of Impact Engineering, 65, 126-136.*
60. *Ramaswamy, K., Patham, B., Savic, V., & Tripathy, B. (2017). Stable and Accurate LS-DYNA Simulations with Foam Material Models: Optimization of Finite Element Model Parameters. SAE International Journal of Materials and Manufacturing, 10(2), 226-233.*
61. *Szyniszewski, S. T., Smith, B. H., Hajjar, J. F., Schafer, B. W., & Arwade, S. R. (2014). The mechanical properties and modeling of a sintered hollow sphere steel foam. Materials & Design (1980-2015), 54, 1083-1094.*